

# Generative Compositional Augmentations for Scene Graph Prediction

Boris Knyazev<sup>\*,1,2</sup> Harm de Vries<sup>3</sup> Cătălina Cangea<sup>4</sup>  
 Graham W. Taylor<sup>1,2</sup> Aaron Courville<sup>5,6</sup> Eugene Belilovsky<sup>5,7</sup>

<sup>1</sup>School of Engineering, University of Guelph <sup>2</sup>Vector Institute for Artificial Intelligence

<sup>3</sup>Element AI <sup>4</sup>University of Cambridge <sup>5</sup>Mila <sup>6</sup>Université de Montréal <sup>7</sup>Concordia University

## Abstract

Inferring objects and their relationships from an image in the form of a scene graph is useful in many applications at the intersection of vision and language. In this work, we consider a challenging problem of compositional generalization that emerges in this task due to a long tail data distribution. Current scene graph generation models are trained on a tiny fraction of the distribution corresponding to the most frequent compositions, e.g. <cup, on, table>. However, test images might contain zero- and few-shot compositions of objects and relationships, e.g. <cup, on, surfboard>. Despite each of the object categories and the predicate (e.g. ‘on’) being frequent in the training data, the models often fail to properly understand such unseen or rare compositions. To improve generalization, it is natural to attempt increasing the diversity of the training distribution. However, in the graph domain this is non-trivial. To that end, we propose a method to synthesize rare yet plausible scene graphs by perturbing real ones. We then propose and empirically study a model based on conditional generative adversarial networks (GANs) that allows us to generate visual features of perturbed scene graphs and learn from them in a joint fashion. When evaluated on the Visual Genome dataset, our approach yields marginal, but consistent improvements in zero- and few-shot metrics. We analyze the limitations of our approach indicating promising directions for future research.

## 1. Introduction

Reasoning about the world in terms of objects and relationships between them is an important aspect of human and machine cognition [21]. In our environment, we can often observe frequent compositions such as “person on a surfboard” or “person next to a dog”. When we are faced with a rare or previously unseen composition such as “dog on a surfboard”, to understand the scene we need to under-

<sup>\*</sup>This work was partially done while the author was an intern at Mila. Correspondence to: bknayazev@uoguelph.ca

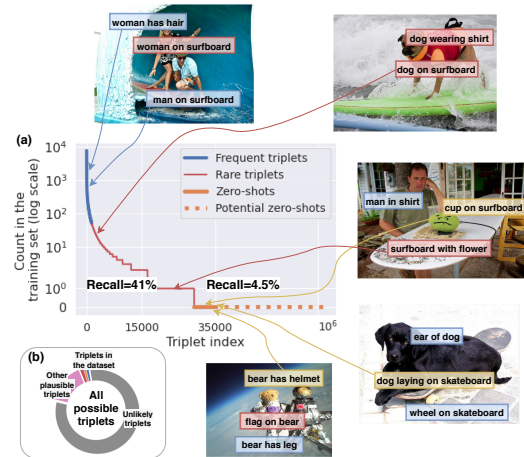


Figure 1. (a) The triplet distribution in Visual Genome [38] is extremely long-tailed, with numerous few- and zero-shot compositions (highlighted in red and yellow respectively). (b) The training set contains a tiny fraction (3%) of all possible triplets, while many other plausible triplets exist. We aim to “hallucinate” such compositions using GANs to increase the diversity of training samples and improve generalization. Recall results are from [65].

stand the concepts of ‘person’, ‘dog’, ‘surfboard’ and ‘on’. While such unbiased reasoning about concepts is easy for us humans, for machines this task has remained extremely challenging [3, 32, 4, 35, 40]. Learning-based models tend to capture spurious statistical correlations in the training data [2, 50], e.g. ‘person’ rather than ‘dog’ has always occurred on a surfboard. When the evaluation is explicitly focused on *compositional generalization* – ability to recognize novel or rare combinations of objects and relationships – such models then can fail remarkably [3, 45, 65, 36].

Predicting compositions of objects and the relationships between them from images is part of the scene graph generation (SGG) task. The inferred scene graph (SG) [33] can be used directly for downstream tasks at the intersection of vision and language, such as VQA [80, 29, 7, 41, 26, 12], image captioning [75, 22, 42, 69, 46], retrieval [33, 5, 65, 67, 60] and others [1, 72]. Due to a long tail data distribution, the SGG task is challenging, with the inevitable

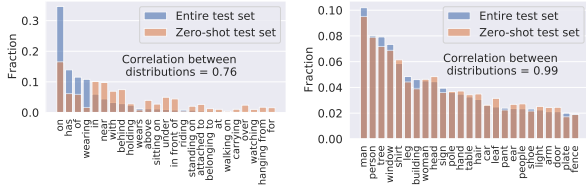


Figure 2. The distributions of top-25 predicate (left) and object (right) categories in Visual Genome [38] (split of [71]).

appearance of zero-shot (ZS) compositions (triplets) of objects and relationships at test time, e.g. “cup on surfboard” (Figure 1). The results using the recent Total Direct Effect (TDE) method [65] show a severe drop in ZS recall highlighting the extreme challenge of compositional generalization. This might appear surprising given that the marginal distributions in the entire scene graph dataset (e.g. Visual Genome [38]) and the ZS subset are very similar (Fig. 2). More specifically, the predicate and object categories that are frequent in the entire dataset, such as ‘on’, ‘has’, ‘of’ and ‘man’, ‘person’, ‘tree’ *also dominate* among the ZS triplets. For example, both “cup on surfboard” and “bear has helmet” consist of frequent entities, but represent extremely rare compositions (Fig. 1). This strongly suggests that the challenging nature of correctly predicting ZS triplets does not directly stem from the imbalance of predicates (or objects), as commonly viewed in the previous SGG works, where the models attempt to improve mean (or predicate-normalized) recall metrics [9, 18, 66, 82, 65, 10, 77, 73]. Therefore, this motivates us to focus on compositional generalization and associated zero- and few-shot metrics.

One approach to tackling this problem in SGG is to explicitly introduce an inductive bias of compositionality. This can take the form of translation operators [81], decoupling object and predicate features [76], constructing causal graphs [65] or, more implicitly, by normalizing the loss [36]. While recent improvements [65, 36] slightly bridge the generalization gap (Figure 3), the state-of-the-art result in zero-shot recall is still 4.5% compared to 41% for non zero-shot (all-shot recall). Furthermore, in certain cases this improvement comes at a drop in other evaluation metrics [65] indicating a trade-off between them.

To address the problem of compositional generalization, we consider another approach. We explore exposing the model to a large diversity of training examples that can lead to emergent generalization [27, 56]. To avoid expensive labeling of additional data, we propose an approach based on conditional generative adversarial networks (GANs) [19, 47]. Our general idea is augmenting the dataset by perturbing scene graphs and corresponding visual features of images, such that together they represent a novel or rare situation.

Overall, we make the following **contributions**:

- We propose SG perturbation methods (§ 3.2.1) as part of a GAN-based model (§ 3.2), to augment the training set with underrepresented compositions;

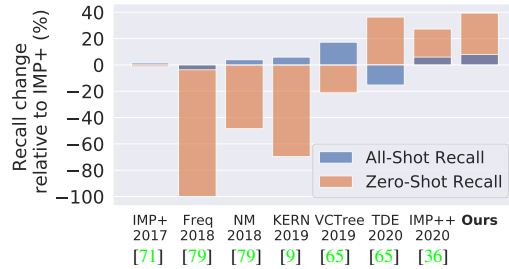


Figure 3. In this work, the compositional augmentations we propose improve on zero-shot (ZS) as well as all-shot recall.

- We propose natural language- and dataset-based metrics to evaluate the quality of (perturbed) SGs (§ 3.3);
- We extensively evaluate our model and outperform a strong baseline in zero-, few- and all-shot recall (§ 4).

Our code is available at <https://github.com/bknyaz/sgg>.

## 2. Related Work

**Scene Graph Generation.** SGG [71] extended an earlier visual relationship detection (VRD) task [45, 58], enabling generation of a complete scene graph (SG) for an image. This spurred more research at the intersection of vision and language, where a SG can facilitate high-level visual reasoning tasks such as VQA [80, 29, 61] and others [53, 1]. Follow-up SGG works [43, 74, 79, 82, 23, 66] have significantly improved the performance in terms of all-shot recall (Fig. 3). While the problem of zero-shot (ZS) generalization was already actively explored in the VRD task [81, 76, 70], in a more challenging SGG task and on a realistic dataset, such as Visual Genome [38], this problem has been addressed only recently in [65] by proposing Total Direct Effect (TDE), in [36] by normalizing the graph loss, and in [63] by the energy-based loss. However, previous SGG works have not addressed the compositional generalization issue by synthesizing rare SGs. The closest work that also considers a generative approach is [70] solving the VRD task. Compared to it, our model follows a standard SGG pipeline and evaluation [71, 79] including object and predicate classification, instead of classifying only the predicate. We also condition a GAN on SGs rather than triplets, which combinatorially increases the number of possible augmentations. To improve SG’s likelihood, we leverage both the language model and dataset statistics as opposed to random compositions as in [70].

**Predicate imbalance and mean recall.** Recent SGG works have shifted the focus to the predicate imbalance problem [9, 18, 66, 82, 65, 10, 77, 44, 78, 73] and mean (over predicates) recall as a metric not sensitive to the dominance of frequent predicates in the test set. However, as we discussed in § 1, the challenge of compositional zero- and few-shot generalization does not directly stem from the

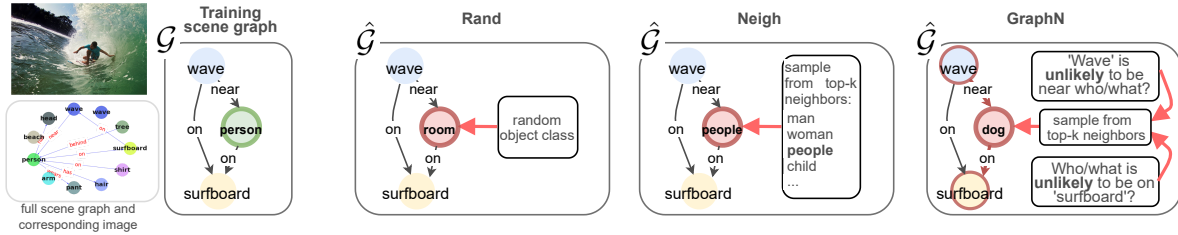


Figure 4. Illustrative examples of different perturbation schemes we consider. Only the subgraph is shown for clarity.

imbalance of predicates, since frequent predicates (e.g. ‘on’) still dominate in unseen/rare triplets (Fig. 2). Moreover, [65] showed mean recall is relatively easy to improve by standard Reweight/Resample methods, while ZS recall is not.

**Data augmentation with GANs** is a standard method for improving performance of machine learning models [55]. Typically these methods rely on domain specific knowledge such as applying known geometric transformations to images [17, 11]. In the case of SGG we require more general augmentation methods, so here we explore a GAN-based approach as one of them. GANs [19] have been significantly improved w.r.t. stability of training and the quality of generated samples [6, 34], with recent works considering their usage for data augmentation [56, 62, 59]. Furthermore, recent work has shown that it is possible to produce plausible out-of-distribution (OOD) examples conditioned on unseen label combinations, by intervening on the underlying graph [37, 8, 64, 13, 20]. In this work, we have direct access to the underlying graphs of images in the form of SGs, which allows us to condition on OOD compositions as in [8, 13].

### 3. Methods

We first provide important notation and definitions (§ 3.1), then describe our GAN-based model (§ 3.2) and the methods to evaluate semantic plausibility of scene graphs (§ 3.3).

#### 3.1. Notation and Definitions

We consider a dataset of  $N$  tuples  $\mathcal{D} = \{(I, \mathcal{G}, B)\}^N$ , where  $I$  is an image with a corresponding *scene graph*  $\mathcal{G}$  [33] and bounding boxes  $B$ . A scene graph  $\mathcal{G} = (O, R)$  consists of  $n$  objects  $O = \{o_1, \dots, o_n\}$ , and  $m$  relationships between them  $R = \{r_1, \dots, r_m\}$ . For each object  $o_i$  there is an associated bounding box  $b_i \in \mathbb{R}^4, B = \{b_1, \dots, b_n\}$ . Each object  $o_i$  is labeled with a particular category  $o_i \in \mathcal{C}$ , while each relationship  $r_k = (i, e_k, j)$  is a triplet with a subject (start node)  $i$ , an object (end node)  $j$  and a predicate  $e_k \in \mathcal{R}$ , where  $\mathcal{R}$  is a set of all predicate classes. For further convenience, we define a categorical triplet (*composition*)  $\tilde{r}_k = (o_i, e_k, o_j)$  consisting of object and predicate categories,  $\tilde{R} = \{\tilde{r}_1, \dots, \tilde{r}_m\}$ . An example of a scene graph is presented in Figure 4 with objects  $O = \{person, surfboard, wave\}$  and relationships  $R = \{(3, above, 1), (1, on, 2)\}$  and categorical relationships  $\tilde{R} = \{(wave, above, person), (person, on, surfboard)\}$ .

#### 3.2. Generative Compositional Augmentations

In a given dataset  $\mathcal{D}$ , such as Visual Genome [38], the distribution of triplets is extremely long-tailed with a small fraction of dominating triplets (Fig. 1). To address the long-tail issue, we consider a GAN-based approach to augment  $\mathcal{D}$  and artificially upsample rare compositions. Our model is based on the high-level idea of generating an additional set  $\hat{\mathcal{D}} = \{(\hat{I}, \hat{\mathcal{G}}, \hat{B})\}^{\hat{N}}$ . A typical scene graph to image generation pipeline is [31]  $\hat{\mathcal{G}} \rightarrow \hat{B} \rightarrow \hat{I}$ . We describe our model accordingly by beginning with constructing  $\hat{\mathcal{G}}$  and  $\hat{B}$  (§ 3.2.1) followed by the generation of  $\hat{I}$  (in our case, features) (§ 3.2.2). The overall generative pipeline is presented in Figure 5.

##### 3.2.1 Scene Graph Perturbations

We propose methods that synthetically increase the presence of underrepresented triplets in the dataset. Our objective is to construct diverse compositions avoiding both very likely (already abundant in the dataset) and very unlikely (“implausible”) combinations of objects and predicates, so that the distribution of synthetic  $\hat{\mathcal{G}}$  will resemble the tail of the real distribution of  $\mathcal{G}$ .

To construct  $\hat{\mathcal{G}}$ , we choose a strategy of perturbing existing SGs available in  $\mathcal{D}$ , since constructing graphs from scratch is more difficult. Our perturbation schemes take a training scene graph  $\mathcal{G}$  and perturb it into  $\hat{\mathcal{G}}$ :  $\mathcal{G} \rightarrow \hat{\mathcal{G}}$  (Fig. 4). We focus on perturbing nodes only as it allows the creation of highly diverse compositions, so  $\hat{\mathcal{G}} = (\hat{O}, R)$ , where  $\hat{O} = \{\hat{o}_1, \dots, \hat{o}_n\}$  are the replacement object categories. However, our methods can be extended for edges too.

**RAND** (random) is the simplest strategy, where for a given node  $i$  we uniformly sample a category  $\hat{o}$  from  $\mathcal{C}$ , so that  $o_i = \hat{o}$ .

**NEIGH** (semantic neighbors) leverages pretrained GloVe word embeddings [52] available for each of the object categories  $\mathcal{C}$ . Thus, given node  $i$  of category  $o_i$  we retrieve the top- $k$  neighbors of  $o_i$  in the embedding space using cosine similarity. We then uniformly sample  $\hat{o}$  from the top- $k$  neighbors replacing  $o_i$  with  $\hat{o}$ .

**GRAPHN** (graph-structured semantic neighbors). RAND and NEIGH do not take into account the graph structure or dataset statistics leading to unlikely or not diverse enough compositions. To alleviate that, we propose the GRAPHN method. Given node  $i$ , we consider all triplets

$\{r_k\}$  in the graph  $\mathcal{G}$  that contain  $i$  as the start or end node, i.e.  $r_k = [(i, e_k, j) \text{ or } (j, e_k, i)]$ . For each such  $r_k$  we then find all possible categorical triplets  $\tilde{r}_c$  in the dataset that satisfy  $\tilde{r}_c = [(o_c, e_k, o_j) \text{ or } (o_j, e_k, o_c)]$ , where  $o_c \in \mathcal{C}$ . We also associate each  $o_c$  with a count  $n_c$  of triplet  $\tilde{r}_c$  in the dataset. In case there are multiple  $\tilde{r}_c$  with  $o_c$ , we take the average of the corresponding  $n_c$ . This way we define a set of possible replacements  $\{o_c, n_c\}$  for node  $i$ . Next, we define unnormalized probabilities  $\hat{p}_c$  based on the inverse frequency  $n_c$ , namely  $\hat{p}_c = 1/n_c$ .

Here, one of our key observations is that depending on the evaluation metric and amount of noise in the dataset, we might want to avoid sampling candidates with very high  $p_c$  (low  $n_c$ ). Therefore, to control for that, we introduce an additional hyperparameter  $\alpha$  that allows to filter out candidates with  $n_c < \alpha$  by setting their  $p_c$  to 0. This way we can trade-off between upsampling rare and frequent triplets. We then normalize  $p_c$  to ensure  $\sum p_c = 1$  and sample  $o' \sim p_c$ . To further increase the diversity, the final  $\hat{o}$  is chosen from the top-k semantic neighbors of  $o'$  as in NEIGH, including  $o'$  itself. Compared to RAND and NEIGH, the GRAPHN strategy directly upsamples required compositions based on the dataset statistics and, at the same time, respects the graph structure.

**Sampling nodes.** For each perturbation strategy, we define the intensity  $L \in \mathbb{R}^{[0,1]}$ , which determines the number  $L \times n$  of nodes for which we change the category. We also found that each scene graph typically has a few central nodes or “hubs”, which are densely connected to other nodes. So, we sample nodes based on their sum of in and out degrees. This way we introduce more novel compositions with fewer perturbations. Note that RAND and NEIGH can perturb all nodes in parallel, while GRAPHN is a sequential procedure, where for each node the perturbation is conditioned on the current state of the (perturbed) graph.

**Bounding boxes.** Since we perturb only a few nodes, for simplicity we assume that the perturbed graph has the same bounding boxes  $B$ :  $\hat{B} = B$ . While one can reasonably argue that object sizes and positions vary a lot depending on the category, i.e. “elephant” is much larger than “dog”, we can often find instances disproving that, e.g. if a toy “elephant” or a drawing of an elephant is present. Empirically we found this approach to work well (please see *Appendix* for the experiments with predicting  $\hat{B}$  conditioned on  $\hat{\mathcal{G}}$ ).

### 3.2.2 Scene Graph to Visual Features

Given perturbed  $(\hat{\mathcal{G}}, \hat{B})$ , the next step in our GAN-based pipeline is to generate visual features (Figure 5). To train such a model, we first need to extract real features from the dataset  $\mathcal{D} = \{(I, \mathcal{G}, B)\}^N$ . Following [71, 79], we use a pretrained and frozen object detector [57] to extract global visual features  $H$  from input images. Then, given  $B$  and  $H$ , we use RoIAlign [24] to extract visual features  $(V, E)$  of nodes and edges, respectively. To extract edge features

between a pair of nodes, the union of their bounding boxes is used [79]. Since we do not update the detector, we do not need to generate images as in scene graph to image models [31], just intermediate features  $\hat{H}, \hat{V}, \hat{E}$ .

**Main scene graph classification model  $F$ .** Given extracted  $(V, E)$ , the main model  $F$  predicts a scene graph  $\mathcal{G} = (O, R)$ , i.e. it needs to correctly assign object labels  $O$  to node features  $V$  and predicate classes  $R$  to edge features  $E$ . For  $F$ , we choose to use Iterative Message Passing (IMP) [71], as it shows stronger compositional generalization capabilities than more sophisticated models subsequently developed [36]. Nonetheless, in principle, our pipeline is not constrained to a particular SGG model.

**Generator  $G$ .** The generator  $G$  follows the architecture of [31]. First, a scene graph  $\hat{\mathcal{G}}$  is processed by a graph convolutional network (GCN) to exchange information between nodes and edges. We found it beneficial to concatenate the node features produced by the GCN with visual features  $V'$ , where  $V'$  are sampled from the set  $\{V_{o_i}\}$  precomputed at the previous stage and  $o_i$  is the category of node  $i$ . By conditioning the generator on visual features, the main task of  $G$  becomes simply to align and smooth the features appropriately, which we believe is easier than generating visual features from the categorical distribution. In addition, the randomness of this sampling step injects noise improving the diversity of generated features. The generated node features and the bounding boxes  $\hat{B}$  are used to construct the layout followed by feature refinement [31] to generate  $\hat{H}$ . Afterwards,  $(\hat{V}, \hat{E})$  are extracted from  $\hat{H}$  the same way as  $(V, E)$ .

**Discriminators  $D$ .** We have independent discriminators for nodes and edges,  $D_{\text{node}}$  and  $D_{\text{edge}}$ , that discriminate real features  $(V, E)$  from fake ones  $(\hat{V}, \hat{E})$  conditioned on their class as per the CGAN [47]. We add a global discriminator  $D_{\text{global}}$  acting on feature maps  $H$ , which encourages global consistency between nodes and edges. Thus,  $D_{\text{node}}$  and  $D_{\text{edge}}$  are trained to match marginal distributions, while  $D_{\text{global}}$  is trained to match the joint distribution. The right balance between these discriminators should enable the generation of realistic visual features conditioned on OOD scene graphs.

**Losses.** To train our generative model, we define several losses. These include the baseline SG classification loss (1) and ones specific to our generative pipeline (2)-(5). The latter are motivated by a CycleGAN [83] and, similarly, consist of the reconstruction and adversarial losses (2)-(5).

We use an improved **scene graph classification loss** from [36], which is a sum of the node cross-entropy loss  $\mathcal{L}^O$  and graph density-normalized edge cross-entropy loss  $\mathcal{L}^R$ :

$$\begin{aligned} \mathcal{L}_{\text{CLS}} &= \mathcal{L}(F(V, E), \mathcal{G}) = \\ &= \mathcal{L}^O(F(V, E), O) + \mathcal{L}^R(F(V, E), R). \end{aligned} \quad (1)$$

To improve  $F$  by training it on augmented features  $(\hat{V}, \hat{E})$ , we define the **reconstruction (cycle-consistency)**

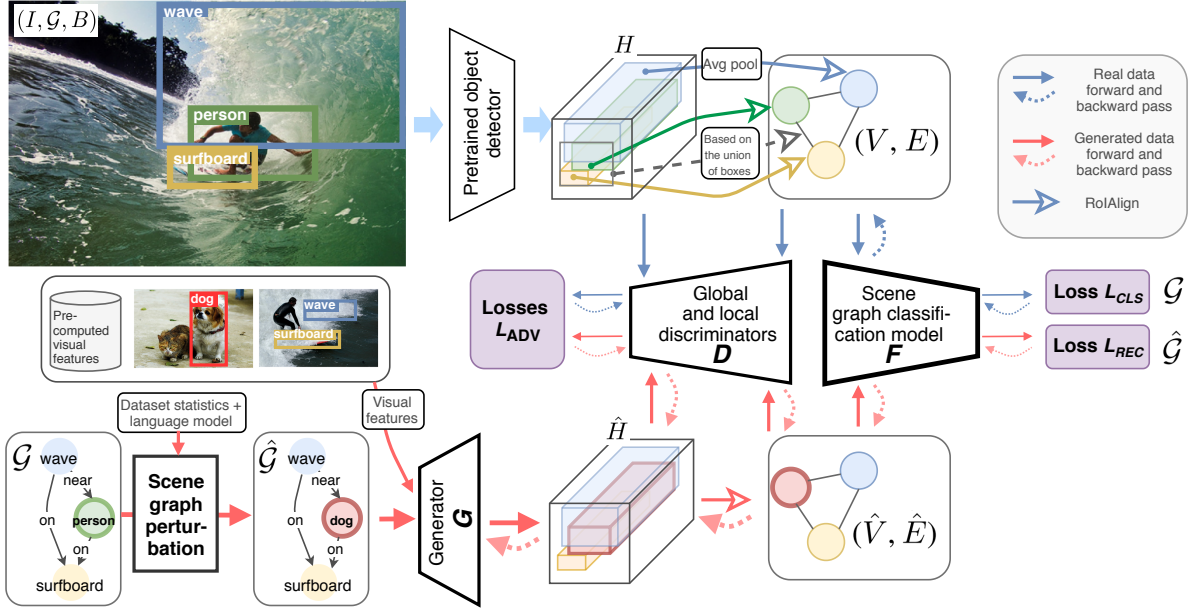


Figure 5. Our generative scene graph augmentation pipeline with its main components: discriminators  $D$ , a generator  $G$  and a scene graph classification model  $F$ . The generator is borrowed from [31] to which we add conditioning on visual features and remove the last convolutional layers producing images. A conditioning class of objects and predicates is passed to the discriminators via CGAN [47], not shown to avoid clutter. Following [54], the discriminators are regularized by having a fully-convolutional architecture with four layers interleaved with ReLU. Global feature maps  $H, \hat{H}$  are  $37 \times 37 \times 512$  dimensional, while node  $V, \hat{V}$  and edge  $E, \hat{E}$  features are  $7 \times 7 \times 512$  dimensional. See §3 for notation.

loss analogous to (1):

$$\begin{aligned} \mathcal{L}_{REC} &= \mathcal{L}(F(G(\hat{G}, \hat{B}, V'), \hat{G})) \\ &= \mathcal{L}^O(F(\hat{V}, \hat{E}), \hat{O}) + \mathcal{L}^R(F(\hat{V}, \hat{E}), R). \end{aligned} \quad (2)$$

We do not update  $G$  on this loss to prevent its potential undesirable collaboration with  $F$ . Instead, to train  $G$  as well as  $D$ , we optimize **conditional adversarial losses** [47]. We first write these separately for  $D$  and  $G$  in a general form. So, for some features  $\mathbf{x}$  and their corresponding class  $\mathbf{y}$ :

$$\begin{aligned} \mathcal{L}_{ADV}^D(\mathbf{x}, \mathbf{y}) &= \mathbb{E}_{\mathbf{x} \sim p_{\text{data}}(\mathbf{x})} [\log D(\mathbf{x}|\mathbf{y})] \\ &\quad + \mathbb{E}_{\hat{\mathbf{G}} \sim p_{\hat{\mathbf{G}}}(\hat{\mathbf{G}})} [\log(1 - D(G(\hat{\mathbf{G}})|\mathbf{y}))] \end{aligned} \quad (3)$$

$$\mathcal{L}_{ADV}^G(\mathbf{y}) = \mathbb{E}_{\hat{\mathbf{G}} \sim p_{\hat{\mathbf{G}}}(\hat{\mathbf{G}})} [\log D(G(\hat{\mathbf{G}})|\mathbf{y})]. \quad (4)$$

We compute these losses for object and edge visual features by using the discriminators  $D_{\text{node}}$  and  $D_{\text{edge}}$ . This loss is also computed for global features  $H$  using  $D_{\text{global}}$ , so that the total discriminator and generator losses are:

$$\begin{aligned} \mathcal{L}_{ADV}^D &= \mathcal{L}_{ADV}^D(V, O) + \mathcal{L}_{ADV}^D(E, R) + \mathcal{L}_{ADV}^D(H, \emptyset) \\ \mathcal{L}_{ADV}^G &= \mathcal{L}_{ADV}^G(O) + \mathcal{L}_{ADV}^G(R) + \mathcal{L}_{ADV}^G(\emptyset), \end{aligned} \quad (5)$$

where  $\emptyset$  denotes that our global discriminator is unconditional for simplicity. Thus, the total loss that we aim to minimize is:

$$\mathcal{L} = \underbrace{\mathcal{L}_{CLS}}_{\text{update } F} + \underbrace{\mathcal{L}_{REC}}_{\text{update } F} - \gamma \left( \underbrace{\mathcal{L}_{ADV}^D}_{\text{update } D} + \underbrace{\mathcal{L}_{ADV}^G}_{\text{update } G} \right), \quad (6)$$

where the loss weight  $\gamma = 5$  worked well in our experiments. Compared to a similar work of [70], in our model all of its components ( $F, D, G$ ) are learned jointly end-to-end. Please

see Appendix for the detailed architectures of  $D$  and  $G$ .

### 3.3. Semantic Plausibility of Scene Graphs

**Language model.** To directly evaluate the quality of perturbations, it is desirable to have some quantitative measure other than downstream SGG performance. We found that a cheap (relative to human evaluation) and effective way to achieve this goal is to use a language model. In particular, we use a pretrained BERT [14] model and estimate the ‘‘semantic plausibility’’ of both ground truth and perturbed scene graphs in the following way. We create a textual query from a scene graph by concatenating all triplets (in a random order). We then mask out one of the perturbed nodes (in case of  $\hat{G}$ ) or a random node (in case of  $G$ ) in the triplet, so that BERT can return (unnormalized) likelihood scores for the object category of the masked out token. We have also considered using this strategy to create SG perturbations as an alternative to GRAPHN. However, we did not find it effective for obtaining rare scene graphs, since BERT is not grounded to visual concepts and not aware of what is considered ‘‘rare’’ in a particular SG dataset. For qualitative evaluation and when BERT scores are averaged over many samples, we found them still useful as a rough measure of SG quality.

**Hit rate.** For perturbed SGs, we compute an additional qualitative metric, which we call the ‘Hit rate’. Assuming we perturbed  $M$  triplets in total for all training SGs, this metric computes the percentage of the triplets matching an actual annotation in a given test subset (zero-, few- or all-shot).

Table 1. Evaluation of generated visual features on the test and test zero-shot sets. The GT test features is the reference distribution. For all metrics, higher is better. The percentage in the superscripts denotes a relative drop of the average metric when switching from test to test-zs conditioning.

		Precision	Recall	Density	Coverage	Avg
nodes	GT test features	0.74	0.75	1.02	0.97	0.87
	GT test-zs features	0.66	0.70	0.99	0.94	0.82 <sup>-6%</sup>
	GAN, test $\mathcal{G}$	0.55	0.42	0.77	0.82	0.64
	GAN, test-zs $\mathcal{G}$	0.47	0.41	0.60	0.75	0.56 <sup>-13%</sup>
edges	GT test features	0.73	0.72	0.97	0.97	0.85
	GT test-zs features	0.53	0.59	0.99	0.87	0.75 <sup>-12%</sup>
	GAN, test $\mathcal{G}$	0.54	0.50	0.59	0.75	0.60
	GAN, test-zs $\mathcal{G}$	0.38	0.50	0.36	0.58	0.46 <sup>-23%</sup>
global	GT test features	0.30	0.31	0.96	0.99	0.64
	GT test-zs features	0.20	0.35	0.73	0.91	0.55 <sup>-14%</sup>
	GAN, test $\mathcal{G}$	0.14	0.22	0.43	0.83	0.41
	GAN, test-zs $\mathcal{G}$	0.11	0.29	0.23	0.68	0.33 <sup>-20%</sup>

## 4. Experiments

### 4.1. Dataset, Models and Hyperparameters

We use a publicly available SGG codebase<sup>1</sup> for evaluation and implementation of Iterative Message Passing (IMP+) [71, 79], which we use as model  $F$ . We use an improved loss from [36], so we denote our baseline as IMP++ (Table 2). We use the default hyperparameters and identical setups for IMP++ and IMP++ with a GAN. We borrow the detector Faster-RCNN with a VGG16 backbone pretrained on Visual Genome from [79] and use it in all our experiments. We evaluate the models on a standard split of Visual Genome [38], with the 150 most frequent object classes and 50 predicate classes, introduced in [71]. The training set has 57723 and the test set has 26446 images. Similarly to [36, 70, 65, 63], in addition to the all-shot (all test scene graphs) case, we define zero-shot, 10-shot and 100-shot test subsets. For each such subset we keep only those triplets in a scene graph that occur 0, 1-10 or 11-100 times during training and remove samples without such triplets, which results in 4519, 9602 and 16528 test scene graphs (and images) respectively. We use a held-out validation set of 5000 images for tuning the hyperparameters.

**Evaluation.** Following prior work [71, 79, 36, 65], we evaluate on two standard SGG tasks: scene graph classification (**SGCls**) and predicate classification (**PredCls**), using recall (R@K) metrics. Unless otherwise stated, we report results with K=100 for SGCls and K=50 for PredCls, since the latter is an easier task with saturated results for K=100. We compute recall without the graph constraint in Table 3, since it is a less noisy metric [36]. We emphasize performance metrics that focus on the ability to recognize rare and novel visual relationship compositions [36, 65, 63]: zero-shot, 10-shot and 100-shot recall. In Tables 3 and 4, the mean and

<sup>1</sup><https://github.com/rowanz/neural-motifs>

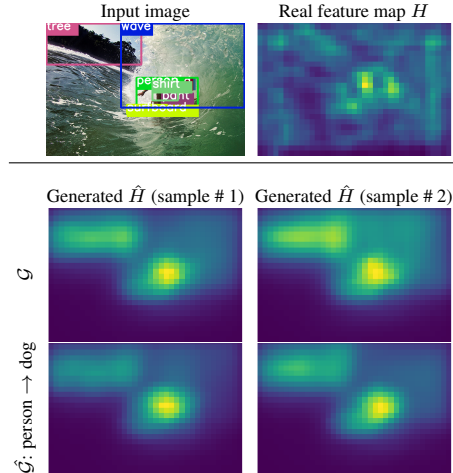


Figure 6. Real  $H$  and Fake (generated)  $\hat{H}$  global feature maps (averaged over the channel dimension) with a perturbation for the triplet “person on surfboard” in  $\mathcal{G}$ .

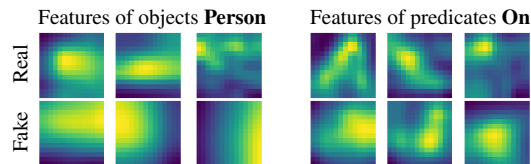


Figure 7. Real and Fake node and edge features (averaged over the channel dimension) for objects and predicates.

Table 2. Two loss variants considered in our experiments.

MODEL	EQ.	LOSS
Baseline (IMP++)	(1)	$\mathcal{L}_{CLS} = \mathcal{L}^O(F(V, E), O) + \mathcal{L}^R(F(V, E), R)$
GAN	(6)	$\mathcal{L} = \mathcal{L}_{CLS} + \mathcal{L}_{REC} - \gamma(\mathcal{L}_{ADV}^D + \mathcal{L}_{ADV}^G)$

standard deviations of 3 runs (random seeds) are reported.

**GAN.** To train the generator  $G$  and discriminators  $D$  of a GAN, we generally follow hyperparameters suggested by SPADE [51]. In particular, we use Spectral Norm [48] for  $D$ , Batch Norm [30] for  $G$ , and TTUR [25] with learning rates of 1e-4 and 2e-4 for  $G$  and  $D$  respectively.

**Perturbation methods hyperparameters.** We found that perturbing  $L = 20\%$  nodes works well across the methods, which we use in all our experiments. For NEIGH we use top-k=10 as a compromise between too limited diversity and plausibility. For GRAPHN, we set top-k=5, as the method enables larger diversity even with very small top-k. To train the models, we use frequency threshold  $\alpha = [2, 5, 10, 20]$ , but for qualitative analysis we use a wider range.

### 4.2. Results

**Evaluation of generated visual features.** We first evaluate the quality of generated node, edge and global features (Table 1) of our trained GAN model (with GRAPHN). For that purpose, we follow [15] and use Precision, Recall [39] and Density, Coverage [49] metrics. We consider two cases: conditioning our GAN on test SGs and zero-shot test (test-zs) SGs. The motivation is similar to [8]: understand if

Table 3. Results on Visual Genome [38] (split of [71]). The top-1 result in each column is **bolded** (ignoring ORACLE-ZS). ORACLE-ZS results are an upper bound estimate of ZS recall obtained by directly using ZS test triplets for perturbations.

MODEL	ZERO-SHOT RECALL		10-SHOT RECALL		100-SHOT RECALL		ALL-SHOT RECALL	
	SGCls	PredCls	SGCls	PredCls	SGCls	PredCls	SGCls	PredCls
Baseline (IMP++ [36])	9.27±0.10	28.14±0.05	21.80±0.19	42.78±0.32	40.42±0.02	67.78±0.07	48.70±0.08	77.48±0.09
GAN+GRAPHN, $\alpha = 2$	<b>9.89</b> ±0.15	28.90±0.14	21.96±0.30	<b>43.79</b> ±0.27	41.22±0.33	69.17±0.24	50.06±0.29	78.98±0.09
GAN+GRAPHN, $\alpha = 5$	9.62±0.29	<b>29.18</b> ±0.33	<b>22.24</b> ±0.11	43.74±0.10	41.39±0.26	69.11±0.05	50.14±0.21	78.94±0.03
GAN+GRAPHN, $\alpha = 10$	9.84±0.17	28.90±0.46	22.04±0.33	43.54±0.36	41.46±0.15	69.13±0.24	50.10±0.23	79.00±0.09
GAN+GRAPHN, $\alpha = 20$	9.65±0.15	28.68±0.28	21.97±0.30	43.64±0.20	41.24±0.08	<b>69.31</b> ±0.17	49.89±0.28	78.95±0.04
<b>Ablated models</b>								
GAN (no perturb.)	9.25±0.20	28.66±0.35	22.15±0.21	43.66±0.29	<b>41.58</b> ±0.20	69.16±0.16	<b>50.38</b> ±0.28	<b>79.05</b> ±0.08
GAN+RAND	9.71±0.09	28.71±0.40	21.89±0.21	43.33±0.18	41.01±0.32	68.88±0.23	49.83±0.32	78.84±0.10
GAN+NEIGH	9.58±0.22	28.63±0.39	21.86±0.23	43.77±0.15	41.14±0.30	69.03±0.09	49.86±0.38	78.89±0.01
<b>ORACLE perturbations <math>\hat{\mathcal{G}}</math></b>								
GAN+ORACLE-ZS $\hat{\mathcal{G}}$	10.11±0.34	29.27±0.10	22.05±0.38	43.78±0.09	41.38±0.50	69.06±0.16	50.19±0.36	79.00±0.08
GAN+ORACLE-ZS $\hat{\mathcal{G}} + \hat{B}$	10.52±0.31	29.43±0.42	21.98±0.39	43.03±0.13	41.12±0.19	68.73±0.17	50.05±0.35	78.65±0.09

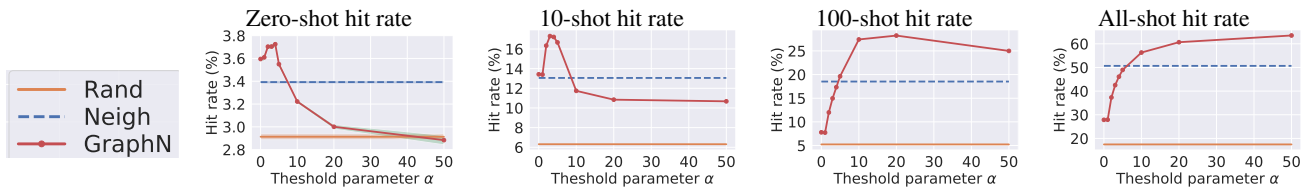


Figure 8. Hit rates on the test subsets using our perturbation methods depending on threshold  $\alpha$  controlling how GRAPHN upsamples triplets.

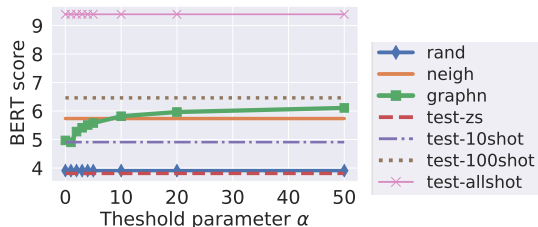


Figure 9. Semantic plausibility (as per BERT) depending on  $\alpha$ . These results should be interpreted with caution, because: (1) the variance of scores is very high (not shown); (2) in the zero- and few-shot test subsets the graphs are significantly smaller, which affects the amount of contextual information available to BERT.

novel compositions confuse the GAN and lead to poor features, that in our context can result in poor training of the main model  $F$ . We also compare the distributions of ground truth (GT) features in the two subsets as an upper bound estimation. In the GT case, all the metrics tend to slightly decrease when we compare test with test-zs as opposed to two subsets of the test distribution. This indicates a large difference between the test and test-zs distributions. In the case of generated features using the GAN, these differences are increased, meaning that indeed it is more challenging to produce good features for a rare composition. Our visual inspection (Fig. 6, 7) complements these results and shows that the generated samples are diverse and respond to the changes in the conditioning. However, the global features generated by our GAN are noticeably more smooth, which might be an effect of the generator’s architectural inductive bias.

We also performed ablations to determine the effect of the

proposed GAN losses (Eq. 6) and other design choices on the SGG performance and the quality of generated features (Figure 11). As a reference model, we use our GAN model without any perturbations. In general, all ablated GANs degrade in performance and feature quality with drops in the latter gracefully correlating with the drops in the former. So by improving generative models in future work, we can expect larger SGG gains. One exception is the GAN without the global terms in Eq. 5, which performed better on zero-shots despite having lower feature quality. This might be explained as some regularization effect. We also found that this model did not combine well with perturbations.

**Main SGG results (Table 3).** We compare the baseline IMP++ to our GAN model trained with different perturbation methods as well as without any perturbations and with so-called ORACLE-ZS perturbations. ORACLE-ZS perturbations are created by directly using ZS triplets from the test set (all obtained triplets are the same as ZS triplets, so that zero-shot hit rate is 100%). ORACLE-ZS +  $\hat{B}$  means that, in addition, each perturbed node uses a bounding box from the sample of the test set, corresponding to the resulted triplet. These results are an upper bound estimate of ZS recall, highlighting the challenging nature of the task.

The GAN without any perturbations significantly outperforms IMP++ on 100-shot and all-shot recalls. This indicates that the GAN might have an implicit inductive bias favoring more frequent scene graphs. This can be related to the feature quality effect we discussed above (Table 1). In particular, the GAN model without perturbations observes rare

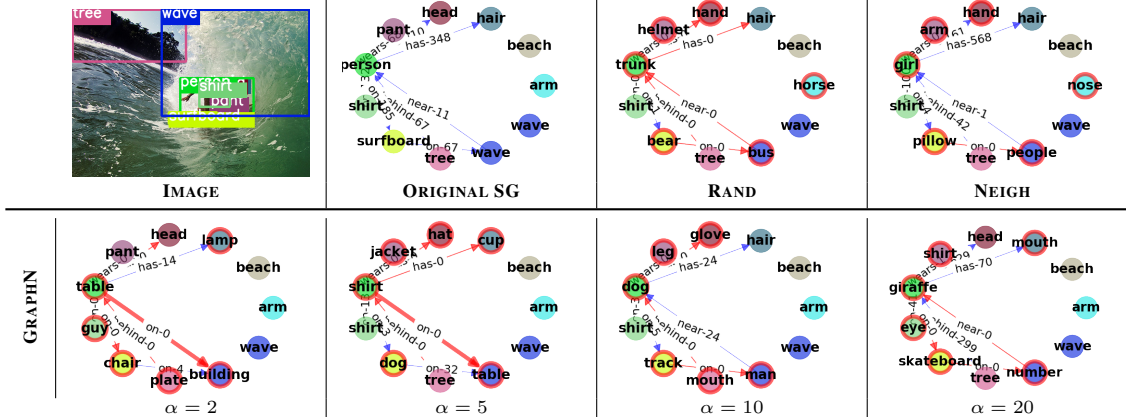


Figure 10. Examples of perturbations (nodes in red) applied to a scene graph  $\mathcal{G}$ . The numbers on edges denote the count of triplets in the training set and a thick red arrow denotes matching a ZS test triplet. See *Appendix* for more examples.

Table 4. ZS recall results compared to previous methods using the graph constraint evaluation. <sup>†</sup>The results are obtained with a more advanced feature extractor and, thus, are not directly comparable.

MODEL	SGCls		PredCls	
	zsR@50	zsR@100	zsR@50	zsR@100
FREQ [79]	0.0	0.0	0.1	0.1
IMP+ [71, 79]	2.5	3.2	14.5	17.2
NM [79]	1.1	1.7	6.5	9.5
KERN [9]	—	1.5	3.9	—
VCtree <sup>†</sup> [65]	1.9	2.6	10.8	14.3
NM <sup>†</sup> [65]	2.2	3.0	10.9	14.5
NM+TDE <sup>†</sup> [65]	3.4	<b>4.5</b>	14.4	18.2
IMP+EBM <sup>†</sup> [63]	3.7	—	18.6	—
IMP++ [36]	3.4	4.2	18.4	21.5
GAN+GRAPHN, avg $\pm$ std	3.7 $\pm$ 0.1	4.4 $\pm$ 0.1	19.1 $\pm$ 0.3	21.8 $\pm$ 0.4
GAN+GRAPHN, max	<b>3.8</b>	<b>4.5</b>	<b>19.5</b>	<b>22.4</b>

compositions rarely and so produces poor features for them (when they appear during training) and stronger features for frequent compositions, increasing the bias of the main model  $F$  to the latter. Next, by adding simple perturbation strategies, RAND (as in [70]) and NEIGH, we obtain improvements on zero-shots, but at a noticeable drop in all other metrics. Both strategies perform similarly.

By using GRAPHN, we further improve ZS results, but also 10-shot and in some cases 100-shot results. We show results for different values of the threshold  $\alpha$  (see § 3.2.1) to indicate the trade-off between metrics. In particular, for lower  $\alpha$  we upsample more of the rare compositions, but compared to RAND and NEIGH these compositions respect the graph structure and dataset statistics. This leads to better ZS results approaching the ORACLE-ZS model. Increasing  $\alpha$  results in upsampling more of the frequent compositions, which generally translates into better 10-shot, 100-shot or all-shot recalls.

Compared to the other previous methods (Table 4), we obtain competitive ZS results on par or better with TDE [65] and recent EBM [63], however it is hard to compare directly due to the different detectors and main models  $F$ , so our

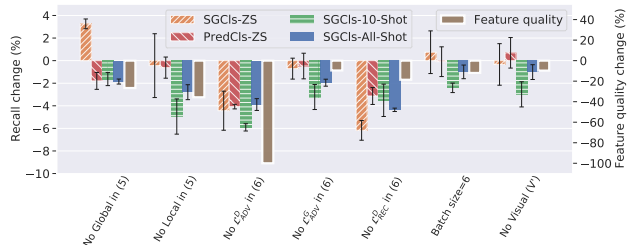


Figure 11. Ablations of our full GAN model without any perturbations on different metrics. Error bars denote standard deviation. Feature quality is measured as the average of Precision, Recall, Density and Coverage on the test-zs subset as in Table 1.

main results in Table 3 are more informative.

**Evaluating the quality of SG perturbations.** We show examples of SG perturbations in Fig. 10 and in *Appendix*. In case of RAND, most of the created triplets are implausible as a result of random perturbations. NEIGH leads to very likely compositions, but less often provides rare plausible compositions. In contrast, GRAPHN can create plausible compositions that are rare or more frequent depending on  $\alpha$ .

We also analyzed the quality of SG perturbations using the metrics proposed in § 3.3: Hit rates (Fig. 8) and BERT-based (Fig. 9). For hit rates, we varied  $\alpha$  of GRAPHN and confirmed that lower  $\alpha$  results in the best hit rate on zero-shots and 10-shots, while larger  $\alpha$  values are better for 100-shot and all-shots. This generally aligns well with the SGG results for different  $\alpha$  in Table 3. Devising a perturbation strategy universally strong across all metrics is challenging and NEIGH can be viewed as such an attempt, which shows average hit rates for all test subsets, but low performance in all SGG metrics. For BERT-based evaluation we estimate the quality of both the GT and perturbed SGs. We found that the overall test set has on average the highest BERT scores, while lower-shot subsets gradually decrease in “semantic plausibility”, which aligns with our intuition. We then perturbed an entire SG of each test sample using dif-

ferent perturbation strategies. Surprisingly, we found that test-zs and completely random SGs have almost the same, very low, plausibility. NEIGH produces SGs of fixed plausibility in between 10-shot and 100-shot. In contrast, with GRAPHN we can gradually slide between these two levels, which helped us to obtain strong SGG results. The BERT scores, however, are not tied to the VG dataset that we used. So, for the same level of semantic plausibility the methods can have quite different hit rates.

### 4.3. Limitations

Our method is limited in three main aspects. **First**, we rely on a pretrained object detector to extract visual features. Without generating augmentations all the way to the images — in order to update the detector on rare compositions — it is hard to obtain significantly stronger performance. While augmentations in the feature space can be effective [16, 68], their adoption for large-scale out-of-distribution generalization is underexplored. **Second**, by making a simplification and keeping GT bounding boxes for perturbed scene graphs, we limit (1) the amount of perturbations we can make (if we permit many nodes to be perturbed, then it is hard to expect the same layout), and (2) the diversity of spatial compositions, which might be an important aspect of compositional generalization. We attempted to verify that using ORACLE-ZS perturbations, which are created by directly using ZS triplets from the test set. Using ORACLE-ZS with GT bounding boxes (our default setting) surprisingly does not result in large improvements. However, when we replace GT boxes with the ones taken from the corresponding samples of the test set, the results improve significantly. This demonstrates that: (1) our GAN model may benefit from reliable bounding box prediction (e.g. [28]); (2) GRAPHN perturbations are already effective (close to ORACLE-ZS) and improving the results further by relying solely on perturbations is challenging. **Third**, the quality of generated features, especially, for novel and rare compositions is currently limited, which is also carefully analyzed in [8]. Addressing this challenge can further improve results both of ORACLE-ZS and non-ORACLE-ZS models.

### 5. Conclusion

We address the SGG task, focusing on the challenging problem of compositional generalization. Our GAN-based augmentations and losses can be added to different existing SGG models and in this work we show an example of combining them with a strong baseline. This generally improves zero-, few- and all-shot results. We found the importance of relying on the structure of scene graphs when performing augmentations as well as the importance of targeting the parameters of augmentations towards a specific metric. Our metrics for evaluating the quality of scene graphs allowed us to inspect different perturbation strategies and further confirm our observations.

### Acknowledgments

This research was developed with funding from DARPA. The views, opinions and/or findings expressed are those of the authors and should not be interpreted as representing the official views or policies of the Department of Defense or the U.S. Government. The authors also acknowledge support from the Canadian Institute for Advanced Research and the Canada Foundation for Innovation. Resources used in preparing this research were provided, in part, by the Province of Ontario, the Government of Canada through CIFAR, and companies sponsoring the Vector Institute: <http://www.vectorinstitute.ai/#partners>.

### References

- [1] Aniket Agarwal, Ayush Mangal, et al. Visual relationship detection using scene graphs: A survey. *arXiv preprint arXiv:2005.08045*, 2020. 1, 2
- [2] Martin Arjovsky, Léon Bottou, Ishaan Gulrajani, and David Lopez-Paz. Invariant risk minimization. *arXiv preprint arXiv:1907.02893*, 2019. 1
- [3] Yuval Atzmon, Jonathan Berant, Bahid Kezami, Amir Globerson, and Gal Chechik. Learning to generalize to new compositions in image understanding. *arXiv preprint arXiv:1608.07639*, 2016. 1
- [4] Dzmitry Bahdanau, Shikhar Murty, Michael Noukhovitch, Thien Huu Nguyen, Harm de Vries, and Aaron Courville. Systematic generalization: what is required and can it be learned? *arXiv preprint arXiv:1811.12889*, 2018. 1
- [5] Eugene Belilovsky, Matthew Blaschko, Jamie Kiros, Raquel Urtasun, and Richard Zemel. Joint embeddings of scene graphs and images. 2017. 1
- [6] Andrew Brock, Jeff Donahue, and Karen Simonyan. Large scale gan training for high fidelity natural image synthesis. *arXiv preprint arXiv:1809.11096*, 2018. 3
- [7] Cătălina Cangea, Eugene Belilovsky, Pietro Liò, and Aaron Courville. VideoNavQA: Bridging the Gap between Visual and Embodied Question Answering. *arXiv preprint arXiv:1908.04950*, 2019. 1
- [8] Arantxa Casanova, Michal Drozdal, and Adriana Romero-Soriano. Generating unseen complex scenes: are we there yet? *arXiv preprint arXiv:2012.04027*, 2020. 3, 6, 9, 15
- [9] Tianshui Chen, Weihao Yu, Riquan Chen, and Liang Lin. Knowledge-embedded routing network for scene graph generation. In *Proceedings of the IEEE Conference on Computer Vision and Pattern Recognition*, pages 6163–6171, 2019. 2, 8, 16
- [10] Vincent S Chen, Paroma Varma, Ranjay Krishna, Michael Bernstein, Christopher Re, and Li Fei-Fei. Scene graph prediction with limited labels. In *Proceedings of the IEEE International Conference on Computer Vision*, pages 2580–2590, 2019. 2
- [11] Ekin D Cubuk, Barret Zoph, Dandelion Mane, Vijay Vasudevan, and Quoc V Le. Autoaugment: Learning augmentation policies from data. *arXiv preprint arXiv:1805.09501*, 2018. 3

- [12] Vinay Damodaran, Sharanya Chakravarthy, Akshay Kumar, Anjana Umaphathy, Teruko Mitamura, Yuta Nakashima, Noa Garcia, and Chenhui Chu. Understanding the role of scene graphs in visual question answering. *arXiv preprint arXiv:2101.05479*, 2021. [1](#)
- [13] Fei Deng, Zhuo Zhi, Donghun Lee, and Sungjin Ahn. Generative scene graph networks. In *International Conference on Learning Representations*, 2021. [3](#)
- [14] Jacob Devlin, Ming-Wei Chang, Kenton Lee, and Kristina Toutanova. Bert: Pre-training of deep bidirectional transformers for language understanding. *arXiv preprint arXiv:1810.04805*, 2018. [5](#)
- [15] Terrance DeVries, Michal Drozdal, and Graham W Taylor. Instance selection for gans. *arXiv preprint arXiv:2007.15255*, 2020. [6](#)
- [16] Terrance DeVries and Graham W Taylor. Dataset augmentation in feature space. *arXiv preprint arXiv:1702.05538*, 2017. [9](#)
- [17] Terrance DeVries and Graham W Taylor. Improved regularization of convolutional neural networks with dropout. *arXiv preprint arXiv:1708.04552*, 2017. [3](#)
- [18] Apoorva Dornadula, Austin Narcomey, Ranjay Krishna, Michael Bernstein, and Li Fei-Fei. Visual relationships as functions: Enabling few-shot scene graph prediction. In *ArXiv*, 2019. [2](#)
- [19] Ian Goodfellow, Jean Pouget-Abadie, Mehdi Mirza, Bing Xu, David Warde-Farley, Sherjil Ozair, Aaron Courville, and Yoshua Bengio. Generative adversarial nets. In *Advances in neural information processing systems*, pages 2672–2680, 2014. [2](#), [3](#)
- [20] Klaus Greff, Raphaël Lopez Kaufman, Rishabh Kabra, Nick Watters, Christopher Burgess, Daniel Zoran, Loic Matthey, Matthew Botvinick, and Alexander Lerchner. Multi-object representation learning with iterative variational inference. In *International Conference on Machine Learning*, pages 2424–2433. PMLR, 2019. [3](#)
- [21] Klaus Greff, Sjoerd van Steenkiste, and Jürgen Schmidhuber. On the binding problem in artificial neural networks. *arXiv preprint arXiv:2012.05208*, 2020. [1](#)
- [22] Jiuxiang Gu, Shafiq Joty, Jianfei Cai, Handong Zhao, Xu Yang, and Gang Wang. Unpaired image captioning via scene graph alignments. In *Proceedings of the IEEE International Conference on Computer Vision*, pages 10323–10332, 2019. [1](#)
- [23] Jiuxiang Gu, Handong Zhao, Zhe Lin, Sheng Li, Jianfei Cai, and Mingyang Ling. Scene graph generation with external knowledge and image reconstruction. In *Proceedings of the IEEE Conference on Computer Vision and Pattern Recognition*, pages 1969–1978, 2019. [2](#)
- [24] Kaiming He, Georgia Gkioxari, Piotr Dollár, and Ross Girshick. Mask r-cnn. In *Proceedings of the IEEE international conference on computer vision*, pages 2961–2969, 2017. [4](#)
- [25] Martin Heusel, Hubert Ramsauer, Thomas Unterthiner, Bernhard Nessler, and Sepp Hochreiter. Gans trained by a two time-scale update rule converge to a local nash equilibrium. In *Advances in neural information processing systems*, pages 6626–6637, 2017. [6](#)
- [26] Marcel Hildebrandt, Hang Li, Rajat Koner, Volker Tresp, and Stephan Günnemann. Scene graph reasoning for visual question answering. *arXiv preprint arXiv:2007.01072*, 2020. [1](#)
- [27] Felix Hill, Andrew Lampinen, Rosalia Schneider, Stephen Clark, Matthew Botvinick, James L. McClelland, and Adam Santoro. Environmental drivers of systematicity and generalization in a situated agent, 2019. [2](#)
- [28] Seunghoon Hong, Dingdong Yang, Jongwook Choi, and Honglak Lee. Inferring semantic layout for hierarchical text-to-image synthesis. In *Proceedings of the IEEE Conference on Computer Vision and Pattern Recognition*, pages 7986–7994, 2018. [9](#)
- [29] Drew Hudson and Christopher D Manning. Learning by abstraction: The neural state machine. In H. Wallach, H. Larochelle, A. Beygelzimer, F. d’Alché Buc, E. Fox, and R. Garnett, editors, *Advances in Neural Information Processing Systems 32*, pages 5903–5916. Curran Associates, Inc., 2019. [1](#), [2](#)
- [30] Sergey Ioffe and Christian Szegedy. Batch normalization: Accelerating deep network training by reducing internal covariate shift. *arXiv preprint arXiv:1502.03167*, 2015. [6](#), [13](#)
- [31] Justin Johnson, Agrim Gupta, and Li Fei-Fei. Image generation from scene graphs. In *Proceedings of the IEEE conference on computer vision and pattern recognition*, pages 1219–1228, 2018. [3](#), [4](#), [5](#), [13](#)
- [32] Justin Johnson, Bharath Hariharan, Laurens van der Maaten, Li Fei-Fei, C Lawrence Zitnick, and Ross Girshick. Clevr: A diagnostic dataset for compositional language and elementary visual reasoning. In *Proceedings of the IEEE Conference on Computer Vision and Pattern Recognition*, pages 2901–2910, 2017. [1](#)
- [33] Justin Johnson, Ranjay Krishna, Michael Stark, Li-Jia Li, David Shamma, Michael Bernstein, and Li Fei-Fei. Image retrieval using scene graphs. In *Proceedings of the IEEE conference on computer vision and pattern recognition*, pages 3668–3678, 2015. [1](#), [3](#)
- [34] Tero Karras, Miika Aittala, Janne Hellsten, Samuli Laine, Jaakko Lehtinen, and Timo Aila. Training generative adversarial networks with limited data. *arXiv preprint arXiv:2006.06676*, 2020. [3](#)
- [35] Daniel Keysers, Nathanael Schärli, Nathan Scales, Hylke Buisman, Daniel Furrer, Sergii Kashubin, Nikola Momchev, Danila Sinopalnikov, Lukasz Stafiniak, Tibor Tihon, et al. Measuring compositional generalization: A comprehensive method on realistic data. *arXiv preprint arXiv:1912.09713*, 2019. [1](#)
- [36] Boris Knyazev, Harm de Vries, Cătălina Cangea, Graham W Taylor, Aaron Courville, and Eugene Belilovsky. Graph density-aware losses for novel compositions in scene graph generation. *British Machine Vision Conference*, 2020. [1](#), [2](#), [4](#), [6](#), [7](#), [8](#), [13](#), [16](#)
- [37] Murat Kocaoglu, Christopher Snyder, Alexandros G Dimakis, and Sriram Vishwanath. CausalGAN: Learning causal implicit generative models with adversarial training. *arXiv preprint arXiv:1709.02023*, 2017. [3](#)
- [38] Ranjay Krishna, Yuke Zhu, Oliver Groth, Justin Johnson, Kenji Hata, Joshua Kravitz, Stephanie Chen, Yannis Kalan-

- tidis, Li-Jia Li, David A Shamma, et al. Visual genome: Connecting language and vision using crowdsourced dense image annotations. *International Journal of Computer Vision*, 123(1):32–73, 2017. 1, 2, 3, 6, 7, 13, 14
- [39] Tuomas Kynkäänniemi, Tero Karras, Samuli Laine, Jaakko Lehtinen, and Timo Aila. Improved precision and recall metric for assessing generative models. *arXiv preprint arXiv:1904.06991*, 2019. 6
- [40] Brenden M Lake. Compositional generalization through meta sequence-to-sequence learning. In *Advances in Neural Information Processing Systems*, pages 9788–9798, 2019. 1
- [41] Soohyeong Lee, Ju-Whan Kim, Youngmin Oh, and Joo Hyuk Jeon. Visual question answering over scene graph. In *2019 First International Conference on Graph Computing (GC)*, pages 45–50. IEEE, 2019. 1
- [42] Xiangyang Li and Shuqiang Jiang. Know more say less: Image captioning based on scene graphs. *IEEE Transactions on Multimedia*, 21(8):2117–2130, 2019. 1
- [43] Yikang Li, Wanli Ouyang, Bolei Zhou, Kun Wang, and Xiaogang Wang. Scene graph generation from objects, phrases and region captions. In *Proceedings of the IEEE International Conference on Computer Vision*, pages 1261–1270, 2017. 2
- [44] Xin Lin, Changxing Ding, Jinquan Zeng, and Dacheng Tao. Gps-net: Graph property sensing network for scene graph generation. In *Proceedings of the IEEE/CVF Conference on Computer Vision and Pattern Recognition*, pages 3746–3753, 2020. 2, 15
- [45] Cewu Lu, Ranjay Krishna, Michael Bernstein, and Li Fei-Fei. Visual relationship detection with language priors. In *European conference on computer vision*, pages 852–869. Springer, 2016. 1, 2
- [46] Victor Milewski, Marie-Francine Moens, and Iacer Calixto. Are scene graphs good enough to improve image captioning? *arXiv preprint arXiv:2009.12313*, 2020. 1
- [47] Mehdi Mirza and Simon Osindero. Conditional generative adversarial nets. *arXiv preprint arXiv:1411.1784*, 2014. 2, 4, 5
- [48] Takeru Miyato, Toshiki Kataoka, Masanori Koyama, and Yuichi Yoshida. Spectral normalization for generative adversarial networks. *arXiv preprint arXiv:1802.05957*, 2018. 6, 13
- [49] Muhammad Ferjad Naeem, Seong Joon Oh, Youngjung Uh, Yunjey Choi, and Jaejun Yoo. Reliable fidelity and diversity metrics for generative models. In *International Conference on Machine Learning*, pages 7176–7185. PMLR, 2020. 6
- [50] Yulei Niu, Kaihua Tang, Hanwang Zhang, Zhiwu Lu, Xian-Sheng Hua, and Ji-Rong Wen. Counterfactual vqa: A cause-effect look at language bias. *arXiv preprint arXiv:2006.04315*, 2020. 1
- [51] Taesung Park, Ming-Yu Liu, Ting-Chun Wang, and Jun-Yan Zhu. Semantic image synthesis with spatially-adaptive normalization. In *Proceedings of the IEEE Conference on Computer Vision and Pattern Recognition*, pages 2337–2346, 2019. 6
- [52] Jeffrey Pennington, Richard Socher, and Christopher D Manning. Glove: Global vectors for word representation. In *Proceedings of the 2014 conference on empirical methods in natural language processing (EMNLP)*, pages 1532–1543, 2014. 3
- [53] Moshiko Raboh, Roei Herzig, Jonathan Berant, Gal Chechik, and Amir Globerson. Differentiable scene graphs. In *Proceedings of the IEEE/CVF Winter Conference on Applications of Computer Vision*, pages 1488–1497, 2020. 2
- [54] Alec Radford, Luke Metz, and Soumith Chintala. Unsupervised representation learning with deep convolutional generative adversarial networks. *arXiv preprint arXiv:1511.06434*, 2015. 5
- [55] Alexander J Ratner, Henry Ehrenberg, Zeshan Hussain, Jared Dunnmon, and Christopher Ré. Learning to compose domain-specific transformations for data augmentation. In *Advances in neural information processing systems*, pages 3236–3246, 2017. 3
- [56] Suman Ravuri and Oriol Vinyals. Seeing is not necessarily believing: Limitations of biggans for data augmentation. 2019. 2, 3
- [57] Shaoqing Ren, Kaiming He, Ross Girshick, and Jian Sun. Faster r-cnn: Towards real-time object detection with region proposal networks. In *Advances in neural information processing systems*, pages 91–99, 2015. 4
- [58] Mohammad Amin Sadeghi and Ali Farhadi. Recognition using visual phrases. In *CVPR 2011*, pages 1745–1752. IEEE, 2011. 2
- [59] Veit Sandfort, Ke Yan, Perry J Pickhardt, and Ronald M Summers. Data augmentation using generative adversarial networks (cycleGAN) to improve generalizability in ct segmentation tasks. *Scientific reports*, 9(1):1–9, 2019. 3
- [60] Brigit Schroeder and Subarna Tripathi. Structured query-based image retrieval using scene graphs. In *Proceedings of the IEEE/CVF Conference on Computer Vision and Pattern Recognition Workshops*, pages 178–179, 2020. 1
- [61] Jiaxin Shi, Hanwang Zhang, and Juanzi Li. Explainable and explicit visual reasoning over scene graphs. In *Proceedings of the IEEE Conference on Computer Vision and Pattern Recognition*, pages 8376–8384, 2019. 2
- [62] Hoo-Chang Shin, Neil A Tenenholz, Jameson K Rogers, Christopher G Schwarz, Matthew L Senjem, Jeffrey L Gunter, Katherine P Andriole, and Mark Michalski. Medical image synthesis for data augmentation and anonymization using generative adversarial networks. In *International workshop on simulation and synthesis in medical imaging*, pages 1–11. Springer, 2018. 3
- [63] Mohammed Suhail, Abhay Mittal, Behjat Siddiquie, Chris Broaddus, Jayan Eledath, Gerard Medioni, and Leonid Sigal. Energy-based learning for scene graph generation. *arXiv preprint arXiv:2103.02221*, 2021. 2, 6, 8
- [64] Wei Sun and Tianfu Wu. Learning layout and style reconfigurable gans for controllable image synthesis. *arXiv preprint arXiv:2003.11571*, 2020. 3
- [65] Kaihua Tang, Yulei Niu, Jianqiang Huang, Jiaxin Shi, and Hanwang Zhang. Unbiased scene graph generation from biased training. In *Proceedings of the IEEE Conference on Computer Vision and Pattern Recognition*, 2020. 1, 2, 3, 6, 8, 15, 16
- [66] Kaihua Tang, Hanwang Zhang, Baoyuan Wu, Wenhan Luo, and Wei Liu. Learning to compose dynamic tree structures for

- visual contexts. In *Proceedings of the IEEE Conference on Computer Vision and Pattern Recognition*, pages 6619–6628, 2019. 2
- [67] Subarna Tripathi, Sharath Nittur Sridhar, Sairam Sundaresan, and Hanlin Tang. Compact scene graphs for layout composition and patch retrieval. In *Proceedings of the IEEE/CVF Conference on Computer Vision and Pattern Recognition Workshops*, pages 0–0, 2019. 1
- [68] Vikas Verma, Alex Lamb, Christopher Beckham, Amir Najafi, Ioannis Mitliagkas, David Lopez-Paz, and Yoshua Bengio. Manifold mixup: Better representations by interpolating hidden states. In *International Conference on Machine Learning*, pages 6438–6447. PMLR, 2019. 9
- [69] Dalin Wang, Daniel Beck, and Trevor Cohn. On the role of scene graphs in image captioning. In *Proceedings of the Beyond Vision and LANGUAGE: inTEgrating Real-world kNowledge (LANTERN)*, pages 29–34, 2019. 1
- [70] Xiaogang Wang, Qianru Sun, Marcelo ANG, and Tat-Seng CHUA. Generating expensive relationship features from cheap objects. 2019. 2, 5, 6, 8
- [71] Danfei Xu, Yuke Zhu, Christopher B Choy, and Li Fei-Fei. Scene graph generation by iterative message passing. In *Proceedings of the IEEE Conference on Computer Vision and Pattern Recognition*, pages 5410–5419, 2017. 2, 4, 6, 7, 8, 13, 16
- [72] Pengfei Xu, Xiaojun Chang, Ling Guo, Po-Yao Huang, Xiaojiang Chen, and Alexander G Hauptmann. A survey of scene graph: Generation and application. 2020. 1
- [73] Shaotian Yan, Chen Shen, Zhongming Jin, Jianqiang Huang, Rongxin Jiang, Yaowu Chen, and Xian-Sheng Hua. Pcp1: Predicate-correlation perception learning for unbiased scene graph generation. In *Proceedings of the 28th ACM International Conference on Multimedia*, pages 265–273, 2020. 2, 15
- [74] Jianwei Yang, Jiasen Lu, Stefan Lee, Dhruv Batra, and Devi Parikh. Graph r-cnn for scene graph generation. In *Proceedings of the European conference on computer vision (ECCV)*, pages 670–685, 2018. 2
- [75] Xu Yang, Kaihua Tang, Hanwang Zhang, and Jianfei Cai. Auto-encoding scene graphs for image captioning. In *Proceedings of the IEEE Conference on Computer Vision and Pattern Recognition*, pages 10685–10694, 2019. 1
- [76] Xu Yang, Hanwang Zhang, and Jianfei Cai. Shuffle-then-assemble: Learning object-agnostic visual relationship features. In *Proceedings of the European Conference on Computer Vision (ECCV)*, pages 36–52, 2018. 2
- [77] Alireza Zareian, Svebor Karaman, and Shih-Fu Chang. Bridging knowledge graphs to generate scene graphs. In *European Conference on Computer Vision*, pages 606–623. Springer, 2020. 2
- [78] Alireza Zareian, Haoxuan You, Zhecan Wang, and Shih-Fu Chang. Learning visual commonsense for robust scene graph generation. *arXiv preprint arXiv:2006.09623*, 2020. 2
- [79] Rowan Zellers, Mark Yatskar, Sam Thomson, and Yejin Choi. Neural motifs: Scene graph parsing with global context. In *Proceedings of the IEEE Conference on Computer Vision and Pattern Recognition*, pages 5831–5840, 2018. 2, 4, 6, 8, 13, 16
- [80] Cheng Zhang, Wei-Lun Chao, and Dong Xuan. An empirical study on leveraging scene graphs for visual question answering. *arXiv preprint arXiv:1907.12133*, 2019. 1, 2
- [81] Hanwang Zhang, Zawlin Kyaw, Shih-Fu Chang, and Tat-Seng Chua. Visual translation embedding network for visual relation detection. In *Proceedings of the IEEE conference on computer vision and pattern recognition*, pages 5532–5540, 2017. 2
- [82] Ji Zhang, Kevin J Shih, Ahmed Elgammal, Andrew Tao, and Bryan Catanzaro. Graphical contrastive losses for scene graph parsing. In *Proceedings of the IEEE Conference on Computer Vision and Pattern Recognition*, pages 11535–11543, 2019. 2
- [83] Jun-Yan Zhu, Taesung Park, Phillip Isola, and Alexei A Efros. Unpaired image-to-image translation using cycle-consistent adversarial networks. In *Proceedings of the IEEE international conference on computer vision*, pages 2223–2232, 2017. 4

## Appendix

### A. Experimental details

#### A.1. Architectures

For our GAN model see the detailed architectures of the generator and discriminators in Tables 5 and 6 respectively.

Table 5. **Architecture of the generator  $G$ .** All GraphTripleConv and Upsample-Refine blocks include Batch Norm (BN) [30] followed by ReLU/LeakyReLU.  $\tilde{n}$ ,  $\tilde{m}$  are the number of nodes and edges in a batch;  $bs$  is batch size.

Layer	Nodes	Edges
<b>input-1</b> (embedd. layer)	$\tilde{n} \times 200$	$\tilde{m} \times 200$
concat. with boxes $B$	$\tilde{n} \times 204$	$\tilde{m} \times 200$
GraphTripleConv-1	204x64	608x64
GraphTripleConv-2	64x64	192x64
GraphTripleConv-3	64x64	192x64
GraphTripleConv-4	64x64	192x64
GraphTripleConv-5	64x(32·7·7)	192x64
<b>output-1</b>	$\tilde{n} \times 32 \times 7 \times 7$	—
conv1	32x64	
conv2	64x64	
<b>output-2</b>	$\tilde{n} \times 64 \times 7 \times 7$	
<b>input-2:</b> vis. features $V'$	$\tilde{n} \times 512 \times 7 \times 7$	
concatenate	output-2, input-2	
conv3	(64+512)x64	
<b>output-3</b>	$\tilde{n} \times 64 \times 7 \times 7$	
<b>input-3:</b> boxes $B$	$\tilde{n} \times 4$	
Boxes2Layout	build feature maps based on output-3 and $B$	
<b>output-4</b>	$bs \times 64 \times 37 \times 37$	
<b>Global feature maps</b>		
Upsample-Refine-1	64x128	
Upsample-Refine-2	128x256	
Upsample-Refine-3	256x512	
conv1x1	512x512	
<b>output-5</b> ( $\hat{H}$ )	$bs \times 512 \times 37 \times 37$	
RoIAlign	extract node, edge feat. based on output-5 and $B$	
<b>output-6</b> ( $\hat{V}, \hat{E}$ )	$\tilde{n} \times 512 \times 7 \times 7$	$\tilde{m} \times 512 \times 7 \times 7$

In the generator, GraphTripleConvNet<sup>2</sup>, Boxes2Layout<sup>3</sup>, Upsample-Refine<sup>4</sup> are borrowed from the sg2im implementation of [31]. For the baseline IMP++ model we use a publicly available implementation<sup>5</sup> with a default architecture and the graph-normalized loss [36] from another public code<sup>6</sup>.

#### A.2. Hyperparameters and tasks

**SGCls.** We use batch size  $bs = 24$  and  $lr = (1e-3) \times bs$ . Training was done on NVIDIA V100 with 32GB of GPU memory or RTX6000 with 24GB. We train all models for

<sup>2</sup>GraphTripleConvNet: <https://github.com/google/sg2im/blob/master/sg2im/graph.py>

<sup>3</sup>Boxes2Layout: <https://github.com/google/sg2im/blob/master/sg2im/layout.py>

<sup>4</sup>Upsample-Refine: <https://github.com/google/sg2im/blob/master/sg2im/crn.py>

<sup>5</sup>IMP+/IMP++: <https://github.com/rowanz/neural-motifs>

<sup>6</sup>Graph-normalized loss: <https://github.com/bknyaz/sgg>

Table 6. **Architectures of the discriminators  $D$ .** All convolutions are 3x3 without padding and normalized with Spectral Norm (SN) [48].  $\tilde{n}$ ,  $\tilde{m}$  are the number of nodes and edges in a batch;  $bs$  is batch size;  $|C| = 151$ ,  $|\mathcal{R}| = 51$  - number of object and predicate classes including the “background” (no object, no edge) class [79].

Layer	$D_{\text{node}}$	$D_{\text{edge}}$	$D_{\text{global}}$
<b>input</b>	$\tilde{n} \times (512+151) \times 7 \times 7$	$\tilde{m} \times (512+51) \times 7 \times 7$	$bs \times 512 \times 37 \times 37$
real feature/labels	$V, O$	$E, R$	$H$
fake feature/labels	$\hat{V}, \hat{O}$	$\hat{E}, R$	$\hat{H}$
SN-conv1	(512+151)x256	(512+51)x256	512x256
nonlinearity	ReLU	ReLU	LeakyReLU
pooling	—	—	Average-2
SN-conv2	256x128	256x128	256x256
nonlinearity	ReLU	ReLU	LeakyReLU
pooling	—	—	Average-2
SN-conv3	128x64	128x64	256x128
nonlinearity	ReLU	ReLU	LeakyReLU
pooling	—	—	Average-2
SN-conv4	64x1	64x1	128x1
<b>output</b>	$\tilde{n} \times 1$	$\tilde{m} \times 1$	$bs \times 1$

a fixed number of 20 epochs according to [36]. **PredCls** results are obtained following a standard procedure [79] of reusing the SGCls model and setting object classes to ground truth. We use PyTorch  $\geq 1.5$  to train all models. The difference between the graph constraint and no constraint metrics is discussed in [79, 36]. We also report the results on the **SGGen/SGDet** task in § B.6. However, we highlight that SGGen/SGDet is not the focus of our work and we do not expect large improvements, since we do not update the detector on generated features.

### B. Additional experimental results

All presented results in this work are on Visual Genome [38] (split of [71]).

#### B.1. Topk semantic neighbors

In the main text, we used  $\text{topk} = 5$  for GRAPHN and  $\text{topk} = 10$  for NEIGH to allow for the same level of diversity of perturbations in both strategies. To make sure GRAPHN outperforms not just because of a better choice of  $\text{topk}$ , we report results of NEIGH for more values in Table 7. Overall, different values of  $\text{topk}$  do not allow NEIGH to achieve the same level of performance as GRAPHN.

#### B.2. BERT-based evaluation

We show an example of BERT-based evaluation in Fig. 12. In this example, we retrieve the score of 9.8 for the token ‘shorts’ which was masked out in the query. To estimate the overall likelihood of the scene graph we mask out only one node per graph for faster evaluation, which can explain a high variance of SG quality. Aggregating the scores for all nodes should lead to better estimates.

Table 7. Results of GRAPHN with  $\text{topk} = 5$  (same as reported in the main text) compared to NEIGH with different values of  $\text{topk}$ .

MODEL	ZERO-SHOT RECALL		10-SHOT RECALL		100-SHOT RECALL		ALL-SHOT RECALL	
	SGCls	PredCls	SGCls	PredCls	SGCls	PredCls	SGCls	PredCls
GAN+GRAPHN, $\alpha = 2$	9.89 $\pm$ 0.15	28.90 $\pm$ 0.14	21.96 $\pm$ 0.30	43.79 $\pm$ 0.27	41.22 $\pm$ 0.33	69.17 $\pm$ 0.24	50.06 $\pm$ 0.29	78.98 $\pm$ 0.09
GAN+GRAPHN, $\alpha = 5$	9.62 $\pm$ 0.29	29.18 $\pm$ 0.33	22.24 $\pm$ 0.11	43.74 $\pm$ 0.10	41.39 $\pm$ 0.26	69.11 $\pm$ 0.05	50.14 $\pm$ 0.21	78.94 $\pm$ 0.03
GAN+GRAPHN, $\alpha = 10$	9.84 $\pm$ 0.17	28.90 $\pm$ 0.46	22.04 $\pm$ 0.33	43.54 $\pm$ 0.36	41.46 $\pm$ 0.15	69.13 $\pm$ 0.24	50.10 $\pm$ 0.23	79.00 $\pm$ 0.09
GAN+GRAPHN, $\alpha = 20$	9.65 $\pm$ 0.15	28.68 $\pm$ 0.28	21.97 $\pm$ 0.30	43.64 $\pm$ 0.20	41.24 $\pm$ 0.08	69.31 $\pm$ 0.17	49.89 $\pm$ 0.28	78.95 $\pm$ 0.04
GAN+NEIGH, $\text{topk} = 2$	9.43 $\pm$ 0.14	28.65 $\pm$ 0.35	21.75 $\pm$ 0.12	42.90 $\pm$ 0.40	41.25 $\pm$ 0.35	68.63 $\pm$ 0.17	50.00 $\pm$ 0.36	78.79 $\pm$ 0.06
GAN+NEIGH, $\text{topk} = 5$	9.49 $\pm$ 0.21	28.58 $\pm$ 0.40	21.72 $\pm$ 0.23	43.62 $\pm$ 0.05	41.04 $\pm$ 0.26	69.07 $\pm$ 0.09	49.64 $\pm$ 0.29	78.94 $\pm$ 0.11
GAN+NEIGH, $\text{topk} = 10$	9.58 $\pm$ 0.22	28.63 $\pm$ 0.39	21.86 $\pm$ 0.23	43.77 $\pm$ 0.15	41.14 $\pm$ 0.30	69.03 $\pm$ 0.09	49.86 $\pm$ 0.38	78.89 $\pm$ 0.01
GAN+NEIGH, $\text{topk} = 20$	9.65 $\pm$ 0.04	28.57 $\pm$ 0.06	21.82 $\pm$ 0.17	43.28 $\pm$ 0.21	40.98 $\pm$ 0.30	69.01 $\pm$ 0.14	49.68 $\pm$ 0.28	78.92 $\pm$ 0.05

Table 8. Comparison of GAN models using GT versus predicted bounding boxes and ORACLE-ZS perturbations.

MODEL	ZERO-SHOT RECALL		10-SHOT RECALL		100-SHOT RECALL		ALL-SHOT RECALL	
	SGCls	PredCls	SGCls	PredCls	SGCls	PredCls	SGCls	PredCls
GAN+ORACLE-ZS, $\hat{B} = B$	10.11 $\pm$ 0.34	29.27 $\pm$ 0.10	22.05 $\pm$ 0.38	43.78 $\pm$ 0.09	41.38 $\pm$ 0.50	69.06 $\pm$ 0.16	50.19 $\pm$ 0.36	79.00 $\pm$ 0.08
GAN+ORACLE-ZS $\hat{G}$ + test $\hat{B}$	10.52 $\pm$ 0.31	29.43 $\pm$ 0.42	21.98 $\pm$ 0.39	43.03 $\pm$ 0.13	41.12 $\pm$ 0.19	68.73 $\pm$ 0.17	50.05 $\pm$ 0.35	78.65 $\pm$ 0.09
GAN+ORACLE-ZS $\hat{G}$ , pred. $\hat{B}$ (§ B.3)	9.92 $\pm$ 0.13	28.93 $\pm$ 0.63	21.67 $\pm$ 0.36	42.65 $\pm$ 0.47	40.96 $\pm$ 0.48	68.23 $\pm$ 0.28	49.80 $\pm$ 0.50	78.55 $\pm$ 0.14

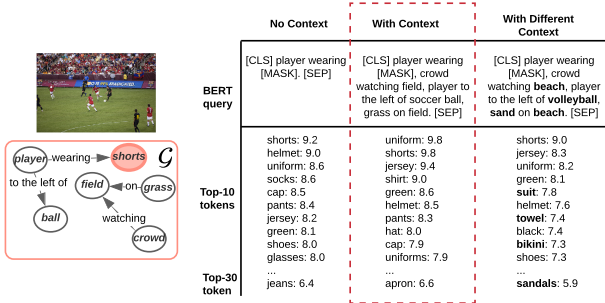


Figure 12. Example of BERT-based evaluation. The evaluation in a dashed rectangle is the one we used in the paper. The other two options are shown for comparison. ‘No context’ returns high scores for implausible tokens, such as ‘glasses’. Using the context is important for more correct evaluation, while changing the context affects the scores accordingly. The scene graph is taken from original Visual Genome [38] for visualization purposes.

### B.3. Learning to predict bounding boxes

In the main text, in our generative pipeline for simplicity we assumed the layout (bounding boxes  $B$ ) is unchanged after perturbing the associated scene graph:  $\hat{B} = B$ . Here, we describe and report results of the alternative version, where the boxes  $\hat{B}$  are predicted by some model  $f$  given a perturbed scene graph  $\hat{B} = f(\hat{G})$ . We borrow the same principle as we used for producing  $\hat{G}$ : instead of producing  $\hat{B}$  from scratch (without relying on  $B$ ), we perturb ground truth  $B$ , so  $\hat{B} = f(\hat{G}, B)$ . This is an easier task, since we only need to predict bounding boxes for part of the scene graph. To achieve that, we train a simple graph convolution network (GCN) to predict a single bounding box  $\hat{b}_i$  given the rest of the layout similar to autoregressive models:  $\hat{b}_i = f(\mathcal{G}, B, i)$ , where the input coordinates of the  $i$ -th object

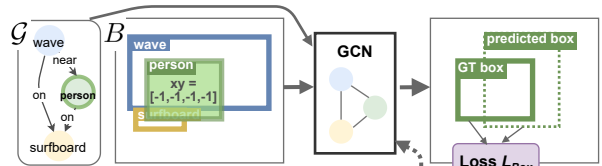


Figure 13. Overview of our model learning to predict bounding boxes, which is used only to report results in the last row of Table 8.

in  $B$  have values  $b_i = [-1, -1, -1, -1]$  (Fig. 13). Our  $f$  is similar to the GCN in our GAN pipeline and is based on GraphTripleConv, but has 3 layers with 64 hidden units and an additional MLP which predicts 4 coordinates of the bounding box. The model is trained with a margin  $l_1$  loss:  $\mathcal{L}_{\text{box}} = \min(0.5S, \max(0.05S, |\hat{b}_i - b_i|_1))$ , where  $S$  is the maximum box coordinate. The idea behind this loss is to avoid having too large or too small penalties making the training more stable given that there is no single correct prediction in this task (i.e. besides the GT there can be many other plausible coordinates).

Table 9. Evaluation of the bounding box prediction model. FD is the Fréchet distance (lower is better). IoU denotes percentage of times the intersection over union between the predicted and GT box is  $\geq 50\%$  (higher is better).

	FD	IoU (%)
	test/test-zs	test/test-zs
No GCN, unconditional (sample GT)	0.001 / 0.001	1.8 / 2.0
GCN, predict $b_i$ (corrupted label in $\mathcal{G}$ )	0.019 / 0.034	2.8 / 2.2
GCN, predict $b_i$	0.018 / 0.037	12.9 / 6.3
GCN, GT $b_i$	$1e-4 / 3e-4$	100 / 100

During training and for evaluation in Table 9, we randomly (uniformly) sample a single object in a scene graph

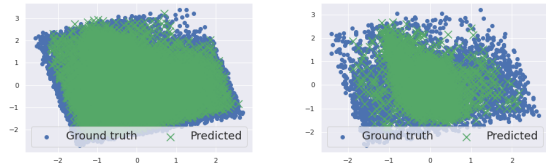


Figure 14. PCA-projected distributions of GT and predicted bounding boxes of the test (left) and test zero-shot (right) sets.

and predict its coordinates given other bounding boxes and a SG. After the model is trained, we sequentially apply it only to perturbed nodes keeping the boxes of non-perturbed nodes unchanged. To isolate the effect of perturbation methods, we evaluate this model using ORACLE-ZS (Table 8). Surprisingly, this model performs worse on all metrics compared to both keeping the layout unchanged and using test bounding boxes.

We estimated the quality of the bounding boxes predicted by our GCN (Table 9). We found that the model respects the conditioning: results of IoU are significantly better compared to the case when we simply sample GT boxes from a distribution for a given class (ignoring SG and other boxes) or when we condition the model on a corrupted (random) label. However, we found that the model performs significantly worse when is fed with ZS compositions. In particular, the distribution appears to be more concentrated around the mean in such cases (Fig. 14). This might explain relatively poor SGG results when we attempt to use the box prediction model in combination with ORACLE-ZS perturbations. Further research is required to resolve the challenges of reliably predicting the layout for rare compositions similarly to [8].

#### B.4. Predicate reweighting and mean recall

[65] showed that mean (over predicates) recall is relatively easy to improve by standard Reweight/Resample methods, while ZS recall is not. To further analyze this and highlight the challenging nature of compositional generalization (targeted in this work) as opposed to predicate imbalance typically targeted in some previous work, we simplify and extend the Reweight idea from [65]. In particular, we compute the frequency  $f_r$  of each predicate class  $r$  in the training set. Then, given a *trained* SGG model, we multiply softmax scores of predicates by  $w^x = 1/f_r^x$ , where  $x$  controls how much we need to balance predicate scores (Fig. 15). We consider  $x = [0, 1, 2, 3]$ , denoting models as  $\times w^x$ , where  $x = 0$  corresponds to not changing predictions (our default setting). The advantage of our post-hoc calibration compared to Reweight [65] is that it does not require retraining the model and allows us to balance performance on frequent and infrequent predicates by carefully choosing  $x$ .

The results indicate a severe trade-off between the mean and all-shot recalls (Table 10). We can achieve very competitive mean recall results by simply using large  $x$ . However,

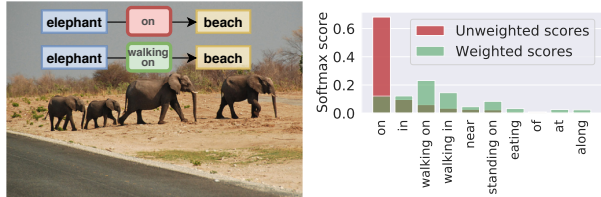


Figure 15. Example of prediction for a zero-shot triplet. Weighting predicate scores increases the score of more descriptive predicates such as 'walking on' compared to 'on', improving mR results, which aligns with [65].

Table 10. Tuning for mean (over predicates) recall versus all-shot recall using our GAN+GRAPHN model (the graph constraint evaluation). Underlined are top results among the variants of our model. <sup>†</sup>The results in [65] are obtained with a more advanced detector and, thus, are not directly comparable.

MODEL	MEAN RECALL		ALL-SHOT RECALL	
	SGCls	PredCls	SGCls	PredCls
GPS-net [44]	12.6	21.3	<b>40.1</b>	<b>66.9</b>
NM <sup>†</sup> [65]	8.5	14.6	39.9	66.0
NM+TDE <sup>†</sup> [65]	14.9	25.5	29.9	46.2
PCPL [73]	<b>19.6</b>	<b>35.2</b>	28.4	50.8
No weighting ( $\times w^0$ )	10.1 $\pm$ 0.2	15.7 $\pm$ 0.3	<u>38.1<math>\pm</math>0.1</u>	<u>62.3<math>\pm</math>0.2</u>
$\times w^1$	14.3 $\pm$ 0.2	22.1 $\pm$ 0.3	35.2 $\pm$ 0.1	56.9 $\pm$ 0.3
$\times w^2$	17.0 $\pm$ 0.1	26.3 $\pm$ 0.1	26.4 $\pm$ 0.4	42.5 $\pm$ 0.2
$\times w^3$	<u>18.3<math>\pm</math>0.1</u>	<u>28.6<math>\pm</math>0.2</u>	17.2 $\pm$ 0.1	27.1 $\pm$ 0.2

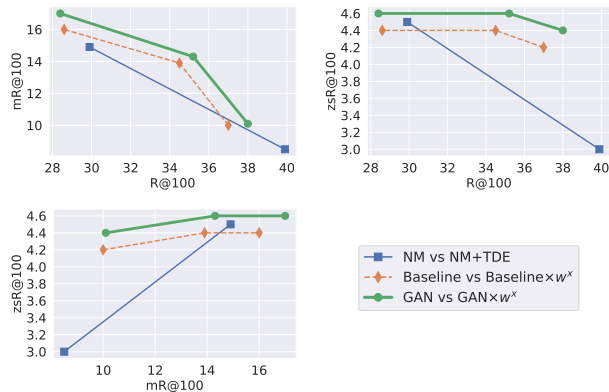


Figure 16. Trade-off between different metrics (R, mR and zsR) in the SGCIs task depending on the strength ( $x = [0, 1, 2]$ ) of weighting predicate scores ( $\times w^x$ ) or using TDE [65].

this dramatically hurts the all-shot recall, potentially leading to invalid predictions, such as “cup walking on table” instead of “cup on table”, as discussed in [73]. Overall, given the three SGG metrics (R, mR and zsR), we observe that (R, mR) and (R, zsR) are two conflicting pairs of metrics, while (mR, zsR) have some correlation (Fig. 16). Clearly, the discussed metrics measure different properties of a given SGG model. In this work, we measure compositional generalization and therefore focus on zero-shot (and closely related few-shot) recall as appropriate metrics for that particular task.

### B.5. Training the baseline longer

In our GAN model we have two loss terms ( $\mathcal{L}_{CLS}$ ,  $\mathcal{L}_{REC}$ ) that update the model  $F$ , which can be considered as having two times more updates compared to the baseline, and so can be an implicit advantage. We investigated if the baseline model can improve itself if it is updated two times more. Our results in Table 11 suggest that the model starts to overfit leading to poor results on all metrics except mean recall. This might indicate that a stronger regularization is required for the baseline trained longer. Our GAN losses can be viewed as such a regularizer leading to better generalization results.

Table 11. Effect of training the baseline model longer. Metrics are R@100 for SGClS and R@50 for PredClS (no graph constraint).

Model	ZERO-SHOT		MEAN RECALL		ALL-SHOT	
	SGClS	PredClS	SGClS	PredClS	SGClS	PredClS
Baseline (IMP++)	9.3±0.1	28.1±0.1	27.8±0.1	33.7±0.3	48.7±0.1	77.5±0.1
Baseline, ×2 updates	8.2	25.8	27.8	35.1	46.6	73.5

### B.6. SGGen/SGDet results

In addition to SGClS/PredClS results presented in the main text, we follow previous work [79, 65] and provide **SGGen** (SGDet) results that rely on using the bounding boxes predicted by the detector as opposed to using GT boxes (Table 12). We follow a standard refinement procedure [79, 36] and fine-tune SGClS models with  $bs = 6$  and  $lr = (1e - 4) \times bs$ . We fine-tune for 2 epochs in all cases, which we set heuristically as our main goal in this task is not to outperform state-of-the-art, but to compare our model with the baseline. During this fine-tuning for simplicity we use only the baseline loss for all models, so that this step’s main purpose is to adapt the SGClS model to predicted bounding boxes instead of ground truth. Despite these simplifications our GAN model still improves on the baseline. However, the results are worse than in previous works, perhaps because: (1) they rely on a stronger detector; (2) we do not update the detector on the generated features conditioned on rare compositions. Addressing these limitations can be the focus of future work. The models with reweighted predicates (§ B.4) significantly improve the results on mean recall (as expected), and interestingly, on one of the zero-shot metrics.

### C. Additional visualizations

Figures 17-19 show additional examples of different perturbations applied to scene graphs from Visual Genome (on top of each figure we show graph  $\mathcal{G}$  along with the corresponding image). Perturbed nodes are highlighted in red. Red edges denote triplets missing both in the training and test sets. Thick red edges denote triplets only present in the test set, i.e. zero-shots. Blue edges denote triplets present in the training set, where the number indicates the total number

Table 12. SGGen results. The top-1 result in each column is **bolded**. †The results in [65] are obtained with a more advanced detector and, thus, are not directly comparable.

MODEL	ZERO-SHOT		MEAN RECALL		ALL-SHOT	
	SGGen zsR@100		SGGen mR@100		SGGen R@100	
	Graph Constraint	✓	✗	✓	✗	✓
FREQ [79, 9, 36]	0.0	0.1	5.6	8.9	27.6	30.9
IMP+ [71, 79, 36]	0.9	0.9	4.8	8.0	24.5	27.4
NM [79, 9, 36]	0.3	0.8	6.1	12.9	30.3	<b>35.8</b>
KERN [9, 36]	0.0	0.0	7.3	<b>16.0</b>	29.8	<b>35.8</b>
VCTree† [65]	0.7	–	6.9	–	36.2	–
NM† [65]	0.2	–	6.8	–	<b>36.9</b>	–
NM+TDE† [65]	<b>2.9</b>	–	9.8	–	20.3	–
Baseline (IMP++ [36])	0.8	0.9	5.9	9.8	25.1	28.1
GAN	1.0	1.2	6.2	10.5	25.4	28.6
GAN×w <sup>2</sup>	1.1	<b>2.2</b>	<b>9.9</b>	15.9	18.5	24.0

of such triplets in the training set. These visualization show that in case of RAND, most of the created triplets are implausible as a result of random perturbations. NEIGH leads to very likely compositions, but less often provides rare plausible compositions. In contrast, GRAPHN can create plausible compositions that are rare or more frequent depending on  $\alpha$ .

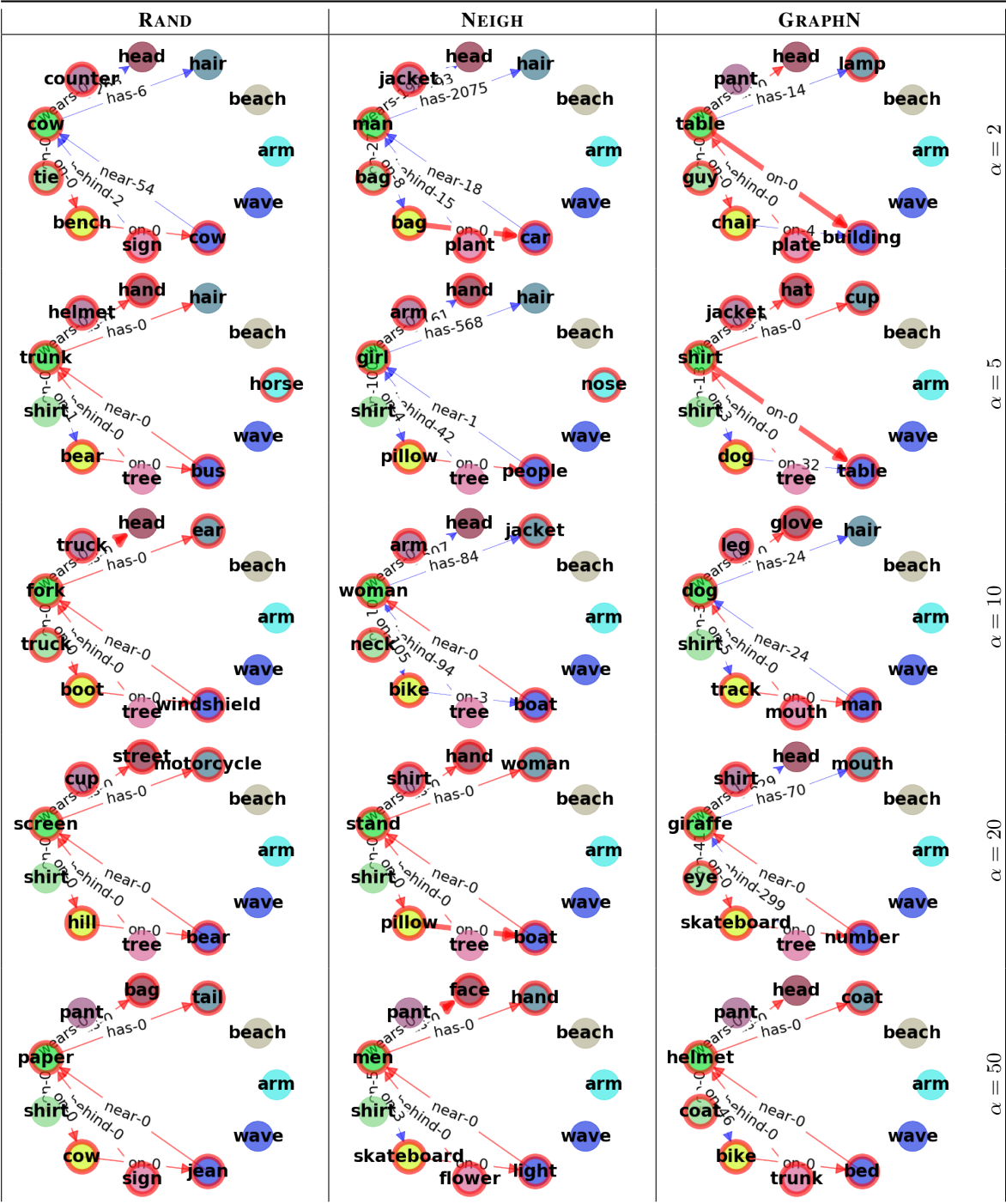
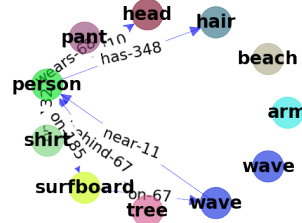
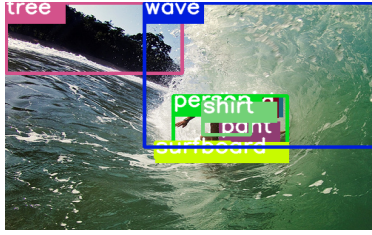


Figure 17. Visualizations of perturbations for image 2350517 from Visual Genome.

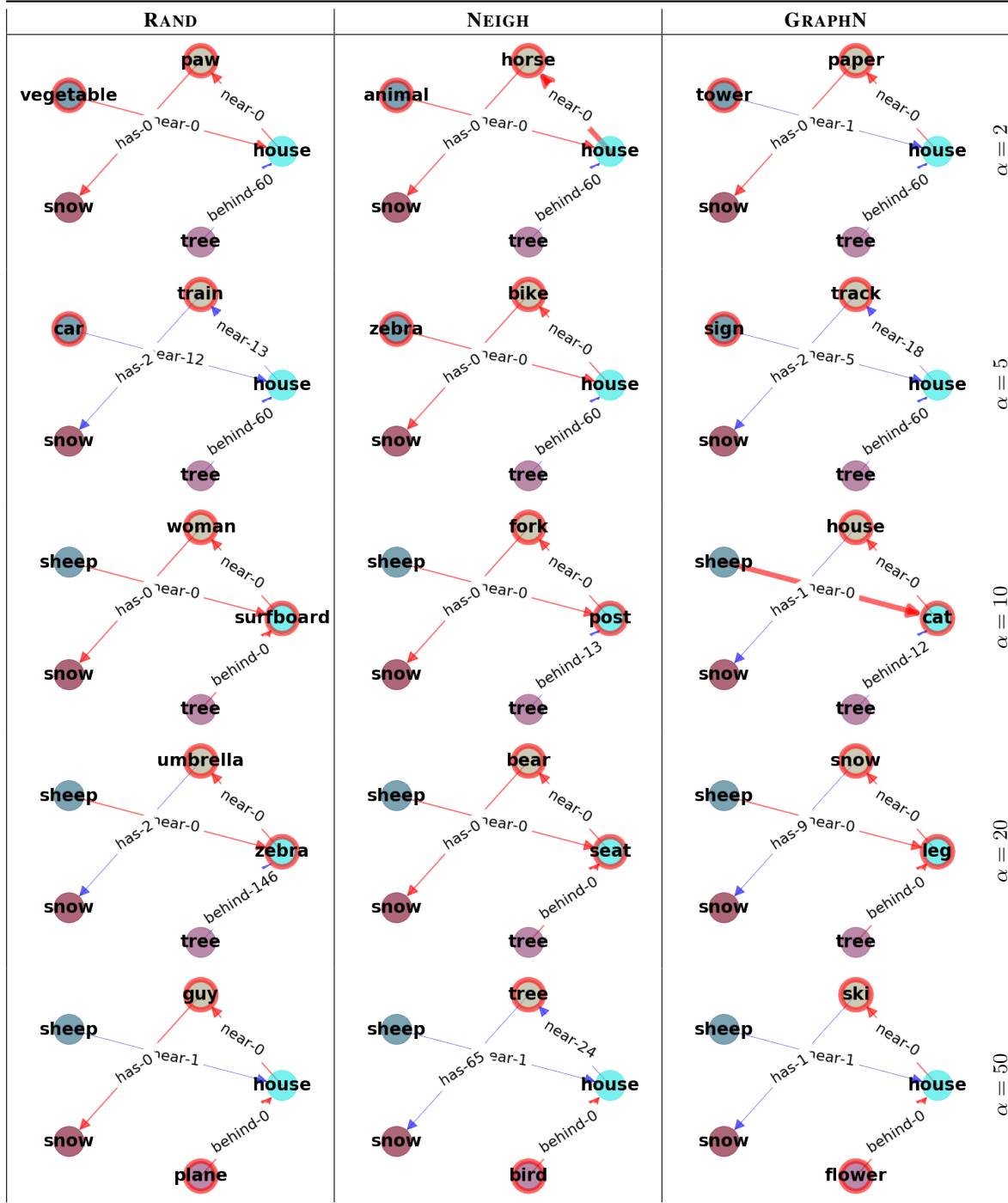
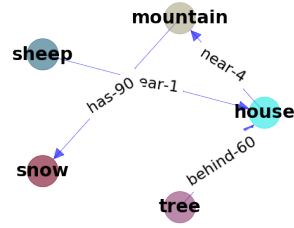


Figure 18. Visualizations of perturbations for image 2343590 from Visual Genome.

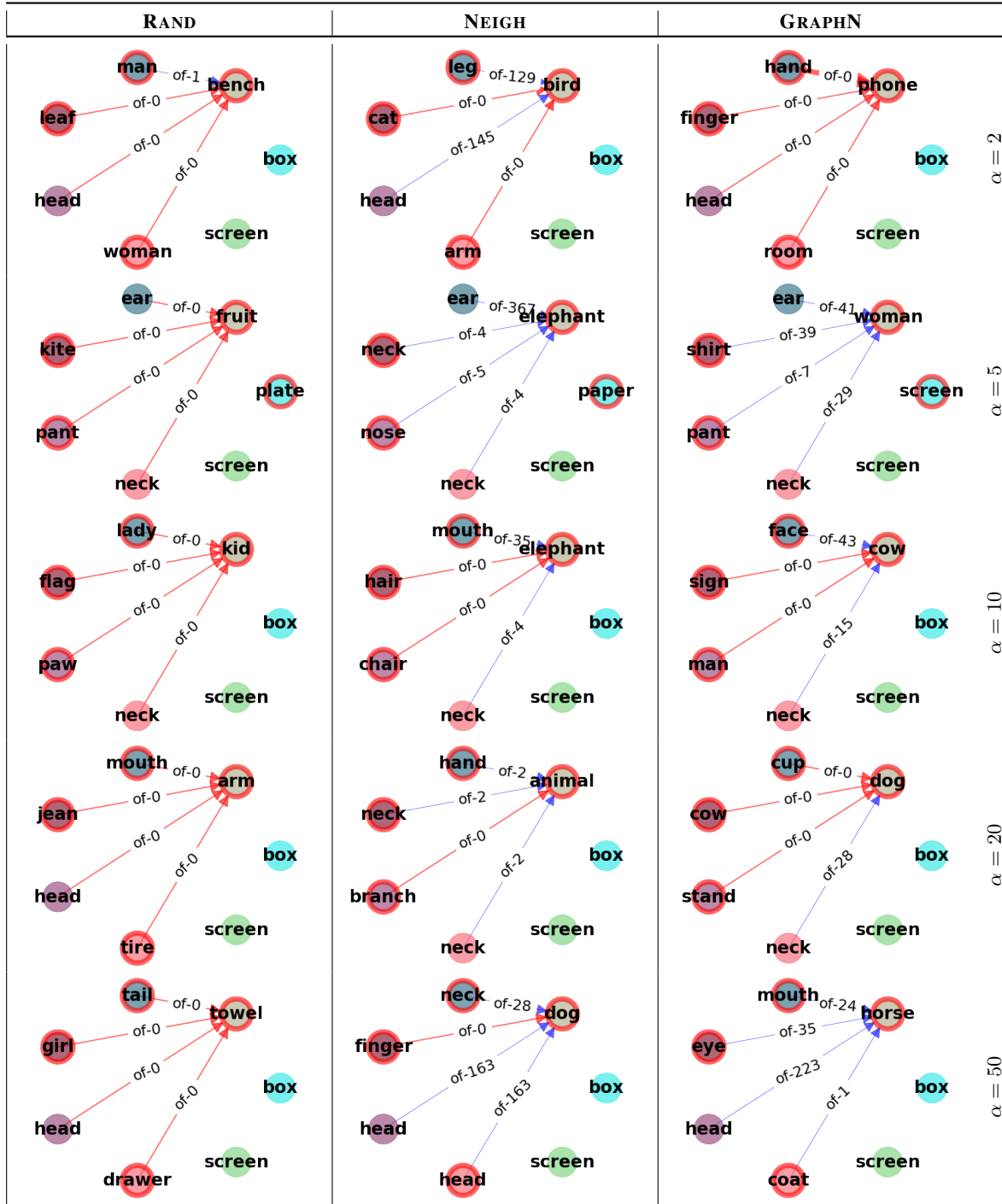
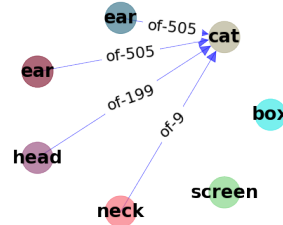


Figure 19. Visualizations of perturbations for image 1159620 from Visual Genome.